ANL/RPG--93/1

DE93 004737

Argonne National Laboratory
9700 South Cass Avenue
Argonne, Illinois 60439

RADIATION AND PHOTOCHEMISTRY SECTION
Annual Report
October 1991 - September 1992
Chemistry Division
Argonne National Laboratory

November 1992

Work performed under the auspices of the Office of Basic Energy Sciences
Division of Chemical Science, U.S. Department of Energy.

RADIATION AND PHOTOCHEMISTRY SECTION

Section Head: Alexander D. Trifunac

Radiation & Photochemistry Group

Group Leader:
Alexander D. Trifunac, Senior Chemist

Staff:
David M. Bartels, Chemist
Charles D. Jonah, Chemist
Yi Lin, Assistant Chemist
Myran C. Sauer, Jr., Chemist
David W. Werst, Assistant Chemist

Postdoctoral Fellows:
Mary Barnabas
Keith Cromack
David M. Loffredo

Special Term Appointees:
Robert H. Lowers
Klaus H. Schmidt
Patricia D. Walsh

Visiting Scientists:
Ron Cooper, University of Melbourne, Melbourne, Australia
6/92 - 7/92
Ping Han, Biomedical Engineering Institute, Tianjin, China
9/87 - 6/92
Vadim V. Krongauz, E. I. du Pont de Nemours and Co. Inc., Wilmington, DE
3/90
An-dong Liu, Radiation Research Centre, Beijing, China
3/90 - Present
Stephen Mezyk, Atomic Energy of Canada, Pinawa, Manitoba Canada
7/92
Paul Percival, Simon Fraser University, Burnaby, British Columbia, Canada
3/92, 10/92

Low-Energy Accelerator Facility (LEAF) Group

Group Leader:
Charles D. Jonah, Chemist

Staff:
Benjamin E. Clifft, Engineering Specialist
George L. Cox, Engineering Specialist
Donald T. Ficht, Engineering Specialist
Allan C. Youngs, Engineering Assistant

TABLE OF CONTENTS

Research Highlights

October 1991 - September 1992

The following survey of the research activities of the Radiation Chemistry and Photochemistry Section is representative of highlights of the past year rather than a comprehensive account. For more detailed accounts of the activities described herein, see the articles listed in *Publications* and *Submissions* at the end of the report, or contact the author(s) indicated.

REACTIVE INTERMEDIATES IN THE CONDENSED PHASE: RADIATION CHEMISTRY AND PHOTOCHEMISTRY

A. D. Trifunac, D. M. Bartels, M. V. Barnabas, K. R. Cromack, C. D. Jonah, Y. Lin, A.-D. Liu, D. M. Loffredo, P. Han, M. C. Sauer, Jr., K. H. Schmidt, D. W. Werst, P. D. Walsh

Outside Collaborators: *R. Cooper, V. V. Krongauz, S. Mezyk, P. W. Percival, E. Roduner, C. Romero*

The research described in this survey represents a multifaceted and comprehensive approach to the study of transient intermediates and chemistry induced by energetic radiation. The goal is to determine the fundamental chemistry that occurs when ionizing or photoionizing radiation interacts with condensed-phase matter. The various short-lived intermediates, radicals, radical ions, electrons, and excited states all play a role in transforming high energy from photons and particles into different stable chemical products.

The simultaneous goals of this research are (1) the understanding of the chemical transformations induced by energetic radiation via the delineation of the overall framework of reactions; (2) the identification and description of reactions of transient species; and (3) the development of novel tools to allow better pursuit of such elusive reaction intermediates. State-of-the-art electron accelerators, ultrafast laser techniques, and novel detection means for the study of ultrafast processes and transient species are continuously being developed and improved.

This survey is presented in two major parts. Part A describes several research efforts in which we study *ions, excited states, and other transients in the condensed phase.* These include studies of radical cations and ion-molecule reactions by the techniques of magnetic resonance, picosecond emission, and picosecond absorption, which probe the role of ions in high-energy chemistry, and studies of ions and their reactivity in specialized matrices such as freons and zeolites.

Part B outlines the work on the *role of solvents in chemical reactivity.* Hydrogen and deuterium atoms have been used as probes of the short-time events in the radiation chemistry of water. The nature of the solvation structure around hydrated electrons has been compared with that of classical monatomic ions by way of thermodynamic and transport properties. In a study in which ions are produced by both laser excitation and pulse radiolysis, we examine the dynamics of solvent reorganization around transient ions.

Highlights of the past year include:

(1) The first observations of aromatic radical anion dimers were made. Dimer formation is hindered by solvation effects, even in nonpolar solvents such as aromatic hydrocarbons.

(2) Significant progress has been made in defining the distribution of spur sizes in the radiolysis of alkane liquids by measuring the time-dependent yields of solute anions, solute triplet states, and solute excited singlet states.

(3) Product studies, including isotopic labeling, and flash photolysis experiments have helped to establish the occurrence of ion-molecule reactions of excited radical ions in photoionization.

(4) The use of zeolite matrices has allowed observation and control of ion-molecule reactions of radical cations.

(5) A combination of experiments, analytical theory, and computer modeling have provided new insights into the structure, energetics, and dynamics of ion solvation in polar liquids.

(6) A careful study of the reaction of H atoms with benzene in water has tested the validity of transition state theory.

(7) Examination of the $(H)_{aq} \rightleftharpoons (e^-)_{aq}$ interconversion reveals that the mechanism is best described as a *proton transfer.* The possibility of proton transfer from Bronsted acids to the solvated electron has implications for other reactions involving this species.

A. Chemistry of Ions in the Condensed Phase

A. D. Trifunac, C. D. Jonah, D. W. Werst, M. C. Sauer, Jr., K. R. Cromack, M. V. Barnabas, D. M. Loffredo, Y. Lin, A.-D. Liu, R. Cooper

1. Structure and Reactivity of Condensed-Phase Radical Ions

A. D. Trifunac, D. W. Werst

The goals of our radical ion studies are to discover the origins and fates of radical ion intermediates in radiation chemical processes, learn the detailed electronic and structural factors that determine radical ion reactivity, and define the role of the medium in ion chemistry. The combined use of pulse radiolysis and time-resolved magnetic resonance techniques is a major strength in this effort because of the versatility of radiolysis for generating radical cations and radical anions and the excellent structural information obtained via magnetic resonance. Radical ions can be unequivocally identified, and many nuances of structure and intermolecular interactions are revealed to increase our understanding of chemical reactivity beyond what can be learned from kinetic studies alone.

Recent studies have revealed that novel types of intermediates are formed by intermolecular interactions between radical ions and solvent molecules or neutral solute molecules. Such interactions are characterized by the open-shell nature of radical ions and are often bonding interactions, that is, covalent bond formation via electronic orbital mixing. In section a, we discuss the formation of rarely observed dimer radical anions. Although radical cations of olefins and aromatic hydrocarbons readily react with their neutral parent molecules to form dimers, the corresponding dimers of the radical anions have been virtually unreported. We have found strong evidence for dimerization of two fluorinated aromatic radical anions. In section b, we explore solvation effects on radical ion reaction mechanisms, in particular, electron transfer and dimer formation, by comparing results in alkane and aromatic hydrocarbon solvents. Related results of a preliminary nature for radical ions in alkene solvents are discussed in section c.

a. Radical Anion Dimers

The octafluoronaphthalene radical anion ($C_{10}F_8^{-\bullet}$) was observed in electron-irradiated dilute solutions by fluorescence-detected magnetic resonance (FDMR). The spectrum observed in n-hexane containing 10^{-3} M $C_{10}F_8$ is shown in Figure 1. This spectrum is described by two quintet coupling constants, a_1 = 23 G and a_2 = 20 G, as appropriate for two sets of four equivalent spin one-half ^{19}F nuclei. What appears as a nine-line spectrum at low resolution clearly separates into the 25-line pattern at slightly higher resolution (expanded view of inner three-line groupings, Figure 1).

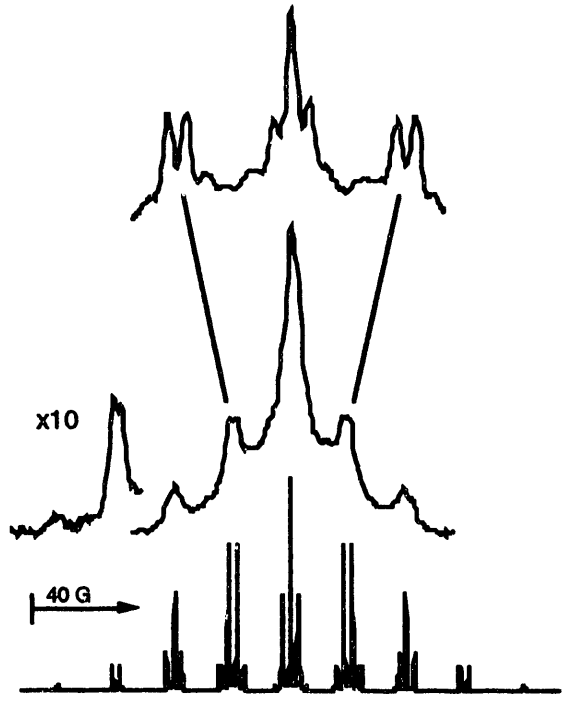

Figure 1. FDMR spectrum observed at 190 K in n-hexane containing 10^{-3} M $C_{10}F_8$ and 10^{-4} M d_{10}-anthracene (lower experimental trace), no d_{10}-anthracene (upper experimental trace). The upper trace was obtained at higher resolution. The stick spectrum was simulated with the parameters, a(4F) = 23 G, a(4F) = 20 G.

Fluorine substituents have a significant effect on the energies of the unoccupied molecular orbitals of aromatic compounds. In a series of fluorine-substituted benzene and pyridine radical anions, it has been shown that fluorine substitution stabilizes the lowest σ^* orbital, destabilizes the lowest π^* orbital, and gives rise to σ^*-π^* crossover. That is, in heavily fluorinated benzene and pyridine radical anions, the

odd electron occupies a delocalized σ* orbital rather than a π* orbital. The main signature of the σ* ground state anion is that the hyperfine splittings are larger for the radical anion than for the radical cation; this ordering is opposite to the behavior found for lightly or unsubstituted aromatic compounds.

The reported coupling constants for $C_{10}F_8^{\bullet+}$ are 19.0 and 4.8 G. Thus, on this basis alone we would conclude that the LUMO of $C_{10}F_8$ is σ*. The relatively small differences between the coupling constants for the cation and anion, however, leave some room for doubt and suggest that the σ* and π* orbitals are close in energy. This finding may explain the small temperature dependence of the hyperfine splittings, for example, if the mixing of the σ* and π* states has a vibronic component. We cannot rule out a predominantly π* ground state with partial σ character from mixing of a nearby σ* state, which might be sufficient to explain the observed coupling constants.

Figure 2 shows how the FDMR spectrum changes with increasing $C_{10}F_8$ concentration. The original spectrum is gradually replaced by a spectrum (Figure 2b) consistent with coupling to 16 nearly equivalent nuclei (a = 7 G). This spectrum is assigned to the dimer radical anion, $(C_{10}F_8)_2^{\bullet-}$, based on the (i) reduced hyperfine splitting, (ii) increased number of equivalent nuclei, (iii) concentration dependence, and (iv) kinetic behavior. By delaying the time window of observation, the ratio of dimer signal to monomer anion signal increases, as monomer anions react with neutral solute molecules to form dimers, equation 1. We propose that $(C_{10}F_8)_2^{\bullet-}$ has a symmetric sandwich-type structure based on the equivalence of the hyperfine couplings.

$$C_{10}F_8^{\bullet-} + C_{10}F_8 \rightleftharpoons (C_{10}F_8)_2^{\bullet-} \qquad (1)$$

Figure 3 illustrates the concentration dependence of the FDMR spectrum of the radical anion derived from 1,2,4,5-tetrafluorobenzene ($C_6H_2F_4$) in n-hexane. Figure 3a shows the inner nine lines of the ($C_6H_2F_4^{\bullet-}$) spectrum (a^{4F} = 41 G, a^{2H} = 5.5 G). The unresolved EPR lines of the anthracene radical ions and the toluene solvent radical cation mask the central triplet of $C_6H_2F_4^{\bullet-}$. Analogous to the behavior observed for $C_{10}F_8$, the $C_6H_2F_4^{\bullet-}$ spectrum disappears with increasing solute concentration and is replaced by a narrower spectrum (Figure 3b). The high-concentration spectrum is not resolved and appears

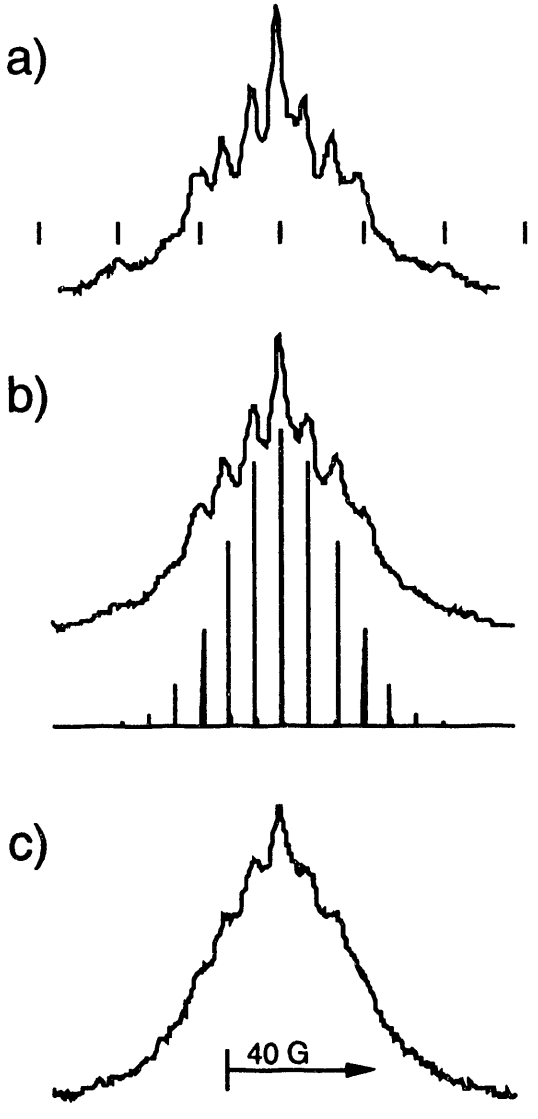

Figure 2. FDMR spectra observed at 200 K in n-hexane containing a) 3×10^{-3} M, b) 5×10^{-3} M, and c) 10^{-2} M $C_{10}F_8$. The markers in a) locate the average positions of the inner seven groups of lines of the $C_{10}F_8^{\bullet-}$ spectrum. The stick spectrum in b) was simulated with a single coupling constant, a(16H) = 7 G.

as shoulders on the central, scintillator ion peak. By analogy to the foregoing example, this is also attributed to formation of a dimer anion radical.

The observation of dimer radical anions is interesting in light of the dearth of previous reports of such species, contrasted with the ease of observation of dimers formed from π radical cations. The only previous example of an anion-molecule dimerization reaction that has been studied by EPR is the tetrafluoroethylene radical anion, which undergoes cyclization with a tetrafluoroethylene molecule to give $c\text{-}C_4F_8^{\bullet-}$.

Radical anions of other ethylenes with strong electron-withdrawing groups are thought to react to form dimers based on optical and kinetic evidence.

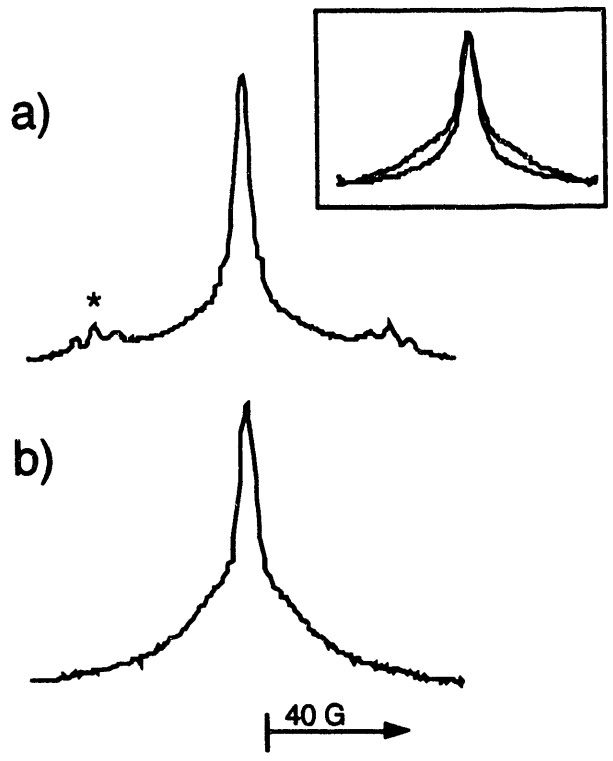

Figure 3. FDMR spectra observed at 190 K in n-hexane containing 10^{-4} M d_{10}-anthracene and a) 10^{-3} M $C_6H_2F_4$, b) 10^{-2} M $C_6H_2F_4$. The inset shows the superposition of the central portions of the same two spectra.

b. Solvent Effects on Radical Ion Reactions: Arene Solvents

The dimer radical anions, $(C_{10}F_8)_2^{\bullet-}$ and $(C_6H_2F_4)_2^{\bullet-}$, observed in n-hexane are not observed in toluene solvent. At low solute concentration (10^{-3} M), the radical anion FDMR spectra are the same in n-hexane and toluene for both $C_{10}F_8^{\bullet-}$ and $C_6H_2F_4^{\bullet-}$. However, the concentration dependence for both anions in toluene is different from that in n-hexane. In the case of $C_{10}F_8^{\bullet-}$, the spectrum is invariant between 10^{-3} and 10^{-1} M; that is, no dimer is formed. Likewise, in the case of $C_6H_2F_4^{\bullet-}$ in toluene, no dimer is formed, and the dependence of the spectrum on concentration indicates the occurrence of the electron self-exchange reaction, equation 2.

$$C_6H_2F_4^{\bullet-} + C_6H_2F_4 \rightleftharpoons C_6H_2F_4 + C_6H_2F_4^{\bullet-} \quad (2)$$

Figure 4 shows an expanded view of one of the H_2 triplets (see asterisk in Figure 3a). As the concentration and exchange rate increase, the lines broaden and the hyperfine splitting decreases. The ^{19}F splitting also decreases. The rate constant for exchange is approximately 10^9 M^{-1} s^{-1}.

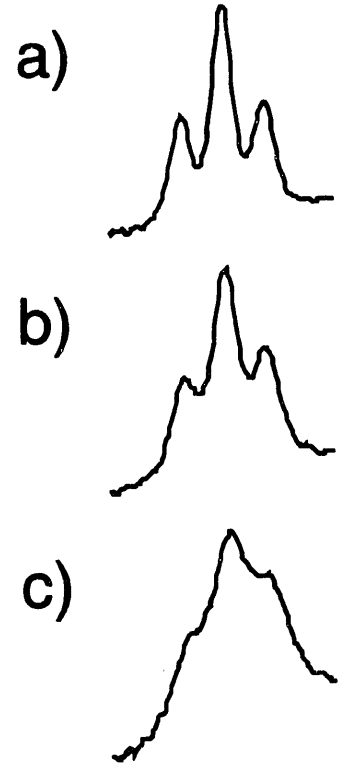

Figure 4. Exchange effects observed for one H_2 triplet in the FDMR spectrum of $C_6H_2F_4^{\bullet-}$. The solvent is toluene; T = 190 K. The $C_6H_2F_4$ concentration was a) 10^{-2} M, b) 3×10^{-2} M, and c) 10^{-1} M.

We conclude that there is a change of mechanism in the arene solvents compared to alkane solvents. Encounters between the radical anions and neutral solute molecules do not produce dimers in toluene; rather, electron exchange is favored. Although evidence for self exchange is not observed for $C_{10}F_8$, our results do not rule out the possibility of exchange. The spectra only indicate that exchange must be slower than the characteristic EPR timescale. The slower exchange rate for $C_{10}F_8$ compared to $C_6H_2F_4$ is consistent with the more positive electron affinity of $C_{10}F_8$, which should increase the activation barrier for electron transfer.

Any solvent effect that impedes close encounter (orbital overlap) of the anion with neutral solute molecules might impede dimer formation, but what solvent effect can explain the difference between the two nonpolar solvents, n-hexane and toluene? We have previously explained the contrasting behavior of thioether *radical cations* in these two solvents based on electron donor-acceptor interactions between toluene solvent molecules and solute radical cations that lead to the formation of solvent radical cation complexes. The FDMR evidence (changes in hyperfine splittings) of spin and charge transfer between solute radical cations and solvent molecules provides a measure of such orbital interactions. However, charge transfer between radical anions and toluene is unfavorable because the donor/acceptor roles are reversed, and toluene is a poor electron acceptor. Consistent with this fact, we observe no significant differences in the anion coupling constants in toluene compared to n-hexane.

Charge transfer from toluene solvent molecules to the neutral solute molecules is more plausible, as charge-transfer complexes between arene solvents and strong electron acceptors have been observed. Ground-state charge-transfer complexes give rise to new absorption bands shifted to longer wavelengths compared to the parent absorption. However, the minimal red shifts observed in the UV spectra of $C_{10}F_8$ and $C_6H_2F_4$ in toluene show that charge transfer to the neutral solutes is very weak.

On the other hand, nonspecific solvation via ion-dipole and ion-induced-dipole interactions between the anions and solvent molecules is not expected to be significantly different in toluene and n-hexane. The dipole moment of n-hexane is near zero, and that of toluene is negligibly small (0.36 D). The polarizabilities of toluene ($\alpha/4\pi\varepsilon_0$ = 12.3 Å^3) and n-hexane ($\alpha/4\pi\varepsilon_0$ = 11.9 Å^3) are also very similar. Perhaps the strength of the anion-solvent interaction is not accurately predicted from the polarizability derived from the refractive index. Nevertheless, the source of the solvent effect remains a puzzle.

The solvent effects in nonpolar solvents described above are not limited to radical anions. A radical cation example that closely parallels the anion study is the tetramethylethylene radical cation ($TME^{\bullet+}$). Like $C_{10}F_8^{\bullet-}$ and $C_6H_2F_4^{\bullet-}$, $TME^{\bullet+}$ reacts with neutral TME solute molecules to form dimer ions (and higher order aggregates) in n-hexane, but not in toluene. We have also ruled out electron donor-acceptor interactions between $TME^{\bullet+}$ and solvent because the EPR parameters of $TME^{\bullet+}$ are the same in n-hexane and toluene.

c. Radical Ions in Alkene Solvents

Preliminary experiments were also carried out in alkenes to characterize their solvent effects on radical ions and radical ion reactions. For example, FDMR spectra of perfluoronaphthalene in 2-methyl-1-butene reveal the formation of $(C_{10}F_8)_2^{\bullet-}$ as in n-hexane. On the other hand, FDMR spectra of TME in 2-methyl-1-butene and 2-methyl-2-butene exhibit slightly reduced (~16%) hyperfine coupling constants. This result is indicative of orbital interactions between the solute radical cations and solvent molecules and suggests electron donation from solvent HOMOs to the $TME^{\bullet+}$ SOMO; that is, similar to our previous observations of solvent complexation of thioether radical cations in arene solvents.

The effect of solvent interactions on the solvent radical cations is an equally important issue. In alkane liquids, this has been difficult to address because the solvent radical cations are very short-lived. In arene solvents, one observes a single narrow line in the spectrum, attributable to the solvent positive ion. This can be interpreted as delocalization of the hole via aggregate cation formation or via electron hopping. Experimental differentiation between the two processes is lacking. In TME, we have observed, for the first time in a pure liquid, a resolved spectrum indicative of a localized solvent radical cation. As found for TME in other alkene solvents, the hyperfine coupling constant for $TME^{\bullet+}$ in pure TME is reduced (~13%) compared to the value in a noninteracting solvent (e.g., n-hexane).

The observation of a localized hole in pure TME is remarkable in light of the proclivity of olefin radical cations to form delocalized aggregates in dilute solutions, equation 3. One wonders if TME is a special

$$TME^{\bullet+} + (TME)_n \rightleftharpoons (TME)_{n+1}^{\bullet+} \qquad (3)$$

case. We have not found another example among several related alkenes. The high symmetry of TME (only one ^1H coupling constant) is a distinct advantage for EPR detection. We plan future experiments to address the relative stabilities of other alkene radical cations to define their ion-molecule reactions with solvent molecules.

No explanation is available at present for the puzzling concentration dependence of tetramethylethylene radical cations, which shows spin delocalization in small clusters and spin localization in large clusters. The behavior of the solvent holes as dictated by the interactions between the solvent radical cations and neutral solvent molecules has far-reaching implications for condensed-phase radiation chemistry. Solvent interactions with the solvent radical cations influence the lifetime, mobility, and oxidizing strength of the solvent hole. These interactions also change the properties, for example, the oxidation potential, of the solvent.

2. Transformations and Reactions of Radical Cations in Zeolites

A. D. Trifunac, M. V. Barnabas

The study of transient radical ions by time-domain methods is closely coupled to the study of such species by matrix-isolation methods. The ability to stabilize radical ions and to control their reactivity is crucial to obtaining a comprehensive overview of their structure and reactivity. We have recently developed zeolites as the matrix of choice. We have shown that the reactions, structures, and electronic states of radical cations can be influenced by the zeolite matrix and experimental parameters, such as substrate loading and temperature.

Radical cations have been studied extensively in various matrices, where a solution of the molecule of interest is prepared and then frozen, or the solute and solvent are codeposited on a low-temperature surface. Matrices stabilize radical cations by separating the geminate electron or anion and the radical cation and by reducing the probability of recombination. Zeolites have the added advantages that they have unique and constrained frameworks and are rigid over a wide temperature range. Thus, while substrate molecules in most frozen matrices are rigidly trapped except very near the melting point of the solvent (usually considerably below room temperature), adsorbed molecules in zeolites explore an open-pore, interconnected surface, the dimensions of which do not change significantly with temperature and which remains rigid well above room temperature. The fact that the volume available in the adsorption site for translational or rotational motion of solutes does not change with temperature has manifold implications for the study and control of radical cation reactivity.

Much of condensed-phase radical cation chemistry is bimolecular: dimerization reactions, ion-molecule reactions, etc. In order to control radical cation reactivity, it is essential to control encounters between radical cations and neutral reactants, the rate of which is normally determined by the concentration and diffusion rate. Zeolites offer more versatility primarily because of the ability to vary substrate mobility more discretely and selectively, by adjusting the pore sizes and temperature. In the limit that a close match is obtained between the size and shape of a cage or channel structure and the substrate species, radical cations can be virtually immobilized in the zeolite matrix. This can greatly enhance radical cation stability, because ion-molecule reactions can only occur in the presence of smaller reactant molecules that are able to diffuse to the adsorption site.

In addition to size restrictions on diffusion, specific guest-host interactions (e.g., electrostatic interactions between radical cations and metal ions of the lattice) can affect radical cation mobility and stability. Adsorption sites that differ in size, shape, polarity, etc., often exist in the same zeolite. This introduces a heterogeneity in the zeolite matrices that does not normally occur in other matrices, and that can lead to a duality of radical cation reactivity within one matrix due to stabilization of different electronic states or different accessibility of adsorption sites. A benefit of the remarkable synthetic versatility of zeolites is that size, shape, and polarity parameters can be varied, allowing one to "tune" the environment to promote or inhibit reactions.

Pentasil-type zeolites (ZSM-5s) are medium-pore-size zeolites, which allow one to monitor primarily the guest-guest or guest-host interactions over a wide temperature range depending on the substrate concentration. Four pentasil zeolites that have approximately the same channel/pore size, but vary in the Si/Al content, and hence the counterion content, were used in our study. This parameter has a significant effect on the reactions of the radical cations.

Radical cations were produced by γ irradiation of solutes in zeolites at 77 K. The radical cations of tetramethylethylene (TME), quadricyclane (Q), and norbornadiene (NBD) were examined by EPR in the zeolites at different temperatures and concentrations. The chemistry of $TME^{\bullet+}$ involves dimerization and ion-molecule reaction, whereas the radical cations $Q^{\bullet+}$ and $NBD^{\bullet+}$ undergo a variety of rearrangements and transformations. The differences in the zeolite interior

surface topology and composition are invoked to explain the new radical cation chemistry.

a. Ion-molecule Reactions: TME

Figure 5 shows the EPR spectra for TME in ZSM-5 after γ irradiation at 77 K with observation at 10 K: (a) 0.1%, (b) 1%, and (c) 7% w/w TME. The spectrum of $TME^{\bullet+}$ consists of 13 lines (11 are observable in Figure 5a) with a hyperfine coupling constant of 17.2 G. When the TME concentration is >5%, the dominant species in the spectrum is the dimer radical cation, $(TME)_2^{\bullet+}$, with a hyperfine coupling constant of 8.3 G. This result is consistent with the formation of dimer radical cations only at higher substrate concentrations. The samples with concentrations between 1 and 5% show that both species are present in different proportions.

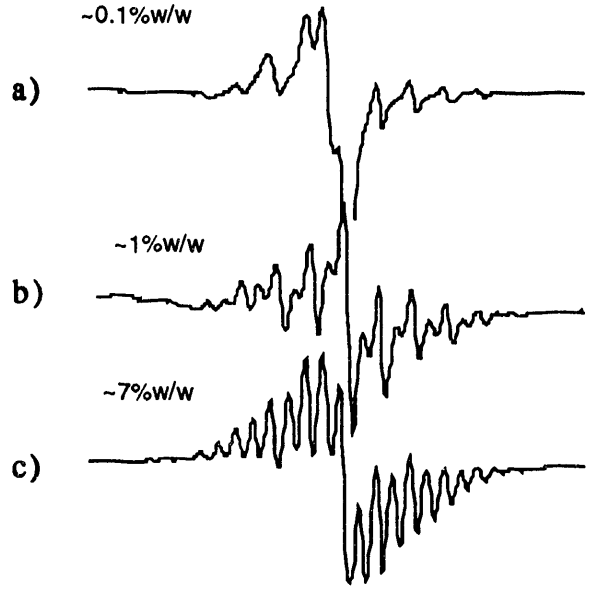

Figure 5 EPR spectra of TME in ZSM-5 at 10 K a) 0.1%, b) ~1%, and c) 7% w/w TME.

EPR spectra recorded for 5% TME in silicalite S115 at 77 K and 110 K are shown in Figure 6. The spectrum at 77 K is clearly due to the monomer radical cation. In the temperature range 90-110 K, the spectral change indicates the formation of a neutral radical through an ion-molecule reaction. At 110 K the dominant species in the spectrum is the trimethylallyl radical. Figure 6c is a simulation of the spectrum of the trimethylallyl radical using the reported hyperfine parameters. Scheme 1 depicts the probable reaction sequence that connects the three TME radical species observed in zeolites.

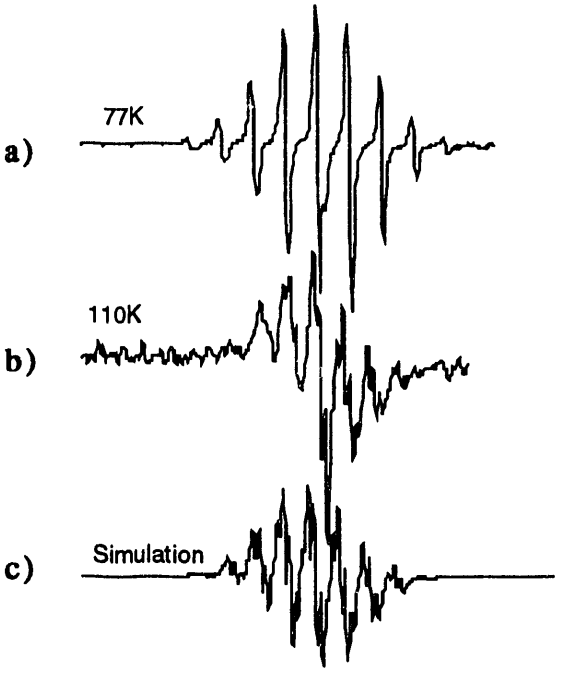

Figure 6. EPR spectra of 5% w/w TME in silicalite a) at 77 K and b) at 110 K. c) is the simulated spectrum of the trimethylallyl radical.

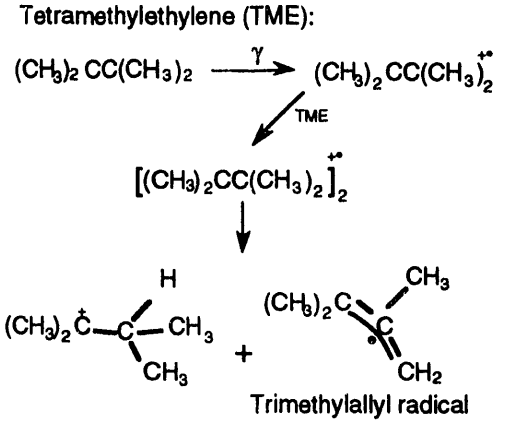

Scheme 1

Figures 5 and 6 offer simple illustrations of the effects of changing the substrate concentration and changing the rate of diffusion via the temperature. However, things can get more complicated. For example, the dimer radical cation formation from the monomer was found to be reversible at low

temperatures. The exact behavior depended on the individual zeolite. Gamma irradiation of TME in Na-ZSM-5 and silicalite S115 gives rise to a dimer radical cation below 50 K, when the concentration of TME is >1% w/w. EPR spectra in the temperature range 50-110 K correspond to the monomer radical cation. Above ~110 K (the exact temperature depending on the TME concentration), only the neutral radical is observed in the case of silicalite, whereas in ZSM-5 both monomer radical cation and neutral radical are observed. EPR spectra in Na-Ω-5 show the coexistence of all three radical species in varying proportions at different temperatures.

Although it is difficult to unravel all of the matrix-specific chemistry, the variations in Si/Al content in these isomorphous zeolites lead to dramatic effects on the radical cation chemistry. These effects include some or all of the following: (1) sites that stabilize $TME^{\bullet+}$ to different extents, (2) different rates of diffusion of TME, (3) different activation barriers for the ion-molecule reaction to form trimethylallyl radical, (4) sites that facilitate dimer cation formation or stabilize $(TME)_2^{\bullet+}$ to different extents. Although it is possible to "tune" radical cation reactivity without a complete understanding of the factors that bear upon the chemistry, greater understanding would allow tuning to be done in a rational and efficient manner.

b. Radical Cation Transformations: Q and NBD

The radical cation chemistry of quadricyclane (Q) and norbornadiene (NBD) is of interest because of the potential utility of this system for energy storage. Previous studies in freon matrices found several conventional and photoinduced radical cation transformations. Scheme 2 gives some of the transformations possible for the radical cations of Q and NBD. Despite vigorous study by several researchers, the reaction mechanism connecting the isomeric species remains elusive. We have undertaken the study of this system in zeolite matrices.

One barrier to solving the Q/NBD system has been the inability to unambiguously distinguish $Q^{\bullet+}$ and $NBD^{\bullet+}$ by EPR. Fast isomerization of $Q^{\bullet+}$ to $NBD^{\bullet+}$ may render the lifetime of $Q^{\bullet+}$ too short to allow observation. On the other hand, calculations indicate that the hyperfine coupling constants for $Q^{\bullet+}$ and $NBD^{\bullet+}$ should be very similar, and we have assumed this to be the case.

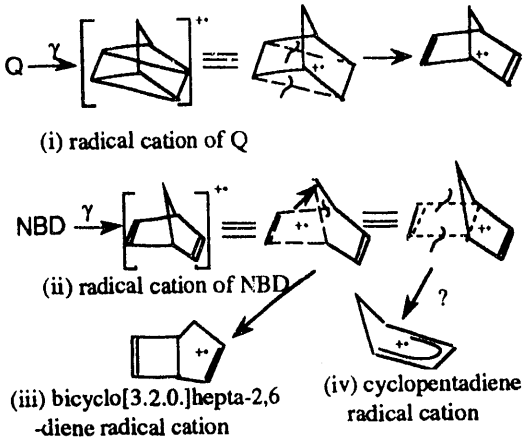

Scheme 2

The EPR spectra for radical cations of Q and NBD (i and ii in Scheme 2) were identical in all of the zeolites, with hyperfine coupling constants: a(4H) = 8.0 G and a(2H) = 3.0 G. They are labeled as (i) and (ii) in the central portions of the spectra in Figures 7 through 9. Figure 7 shows the spectrum observed at 240K for Q (0.07% w/w) in silicalite-S115 (which has the same framework as ZSM-5 with Si:Al > 1000:1). The spectrum was unchanged from 77 K to 290 K.

The rearranged radical cation (iii) in Scheme 2 was not observed in the zeolite with high Al content (Si:Al = 170:1), but it was observed in a narrow temperature range, 100-150 K, in the other three ZSM-5s (Si:Al = 400:1, 980:1, >1000:1) with varying intensity in comparison to the parent radical cation. Figure 8 shows the EPR spectrum observed at 100 K for NBD (0.07% w/w) in ZSM-5 (400:1).

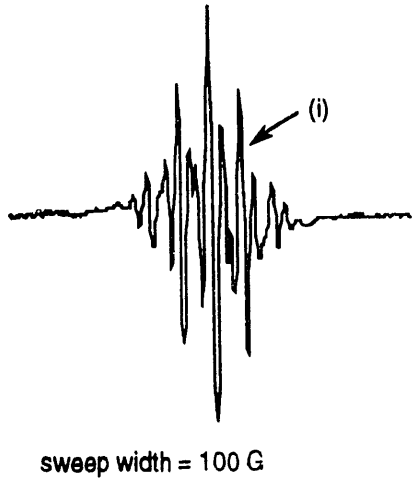

Figure 7. EPR spectrum of quadricyclane (0.07% w/w) in silicalite at 240 K.

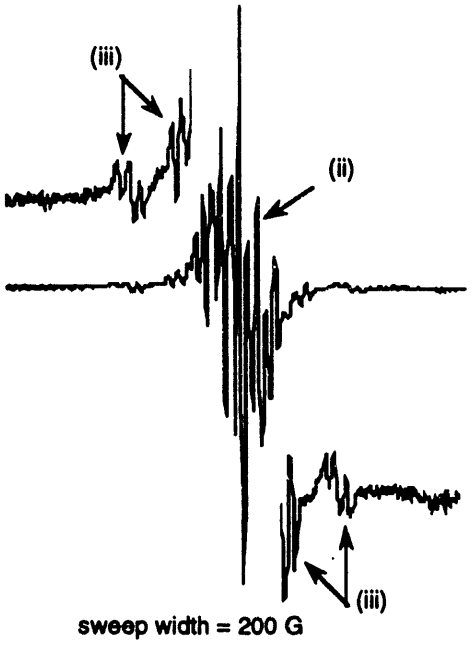

Fig. 8. EPR spectrum of norbornadiene (0.07% w/w) in ZMS-5 (400:1) at 100 K.

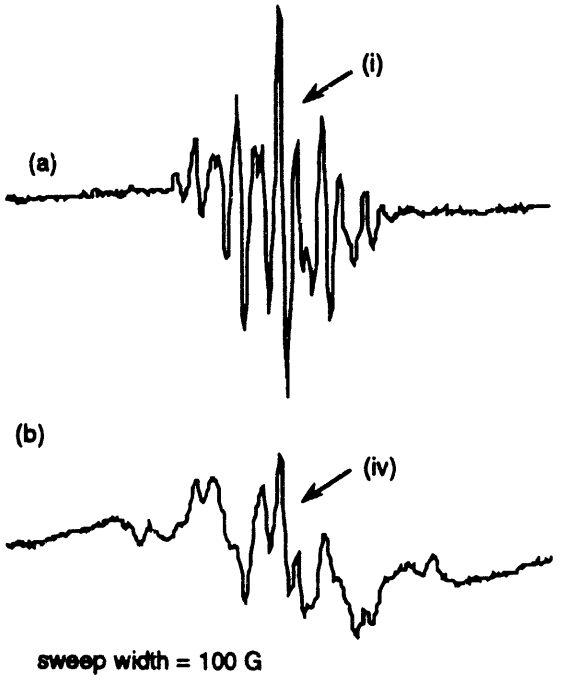

Figure 9. EPR spectra of quadricyclane in ZSM-5 (170:1) at (a) 130 K and (b) 80 K after being warmed to 200 K.

Other species formed by rearrangement (including photoprocesses) and/or deprotonation of $Q^{\bullet+}$ and $NBD^{\bullet+}$ in freon matrices include the cycloheptatrienyl radical cation, toluene radical cation, 7-norbornadienyl radical, and bicyclo(3.2.0)heptadienyl radical. We have observed an additional species in ZSM-5 (170:1), a cycloreversion product, namely cyclopentadienyl radical cation (iv), at temperatures above 200 K. Figure 9 shows (a) the spectrum of $Q^{\bullet+}$ and (b) the spectrum corresponding to the cyclopentadienyl radical cation. The persistence of the parent radical cation spectrum at 200 K eliminates the possibility of the formation of cyclopentadiene before the γ irradiation (i.e., by the catalytic effect of zeolite). A thorough study including the determination of the dependence on concentration, temperature, and time of equilibration (i.e., the time between the adsorption of the solute and the irradiation) is underway.

Our preliminary studies indicate that the diversity and variety of quadricyclane/norbornadiene chemistry in zeolite matrices are quite different than in the conventional freon matrices. We observe many radical cation transformations, which were hitherto observed and/or suggested in the gas phase studies.

3. High-Energy Chemistry

A. D. Trifunac, D. M. Loffredo, A.-D. Liu

The use of intense UV lasers to induce condensed-phase photolysis opens new avenues for the examination of novel photochemistry. When energy input into a condensed-phase system is in excess of that needed to ionize a solute, what happens to the energy excess? Thus far, virtually no work has been done in delineating transient intermediates and products in such "high-energy" regimes. Due to the obvious parallels that can be drawn to radiolysis studies, we have embarked on a comprehensive examination of high-energy chemistry of aromatic molecules in hydrocarbon and alcohol solvents.

Ultraviolet photolysis of an aromatic molecule, AH, in a hydrocarbon or alcohol solvent (RH and ROH) is known to result in ionization, equation 4,

$$AH \xrightarrow{2h\nu} AH^{+\bullet} + e^- \qquad (4)$$

but little is known about other chemical processes and the dependence of these processes on the energy input. Two other processes could result from the excess energy input: homolysis, equation 5, where a

$$AH \sim\sim\sim> AH^{**} \rightarrow A\bullet + H\bullet \quad (5)$$

neutral excited state undergoes homolytic cleavage to yield two radicals, and ion-molecule reaction of an excited radical cation, equations 6-8. It is known that ground state ions, $AH^{+}\bullet$, are quite stable in this regard.

$$AH \sim\sim\sim> AH^{*\bullet+} + e^{-} \quad (6)$$

$$AH^{*\bullet+} + RH \rightarrow A\bullet + RH_2^{+} \quad (7)$$

$$AH^{*\bullet+} + ROH \rightarrow A\bullet + ROH_2^{+} \quad (8)$$

In either instance, the aromatic radical, A•, is formed. Homolysis also yields hydrogen atoms. We can distinguish between these processes by careful examination of reaction products.

Product analysis. When an aromatic molecule in a hydrocarbon or alcohol solution is irradiated with intense UV photons from a pulsed excimer laser at 248 and 308 nm, the solute is consumed. Several products were observed, and their relative yields were determined. The products reveal the formation of the aryl radical (A•) and its subsequent reactions.

In the appropriately isotopically labeled solute and solvent (hydrocarbon), incorporation of H (or D) atoms in the aromatic molecule was detected. Results are given for naphthalene (Table 1 and Scheme 3). These data indicate that the naphthyl radical is formed and that its principal reactions are with the cyclohexane solvent, equation 9, resulting in a series of other

$$A\bullet + RH \rightarrow AH + R\bullet \quad (9)$$

products derived from solvent radicals. All of these products were detected and identified by GC-MS or HPLC-UV methods.

One sees from Table 1 that the extent of product formation is different for different aromatic compounds. More products are formed with higher energy photons, and the product formation is greater in alcohol solutions (Scheme 4).

This last observation is consistent with the ion-molecule reaction, equations 7 and 8, but not with neutral excited state homolysis, equation 5, as one would not expect significant solvent polarity and proton affinity influence on neutral excited state homolysis. However, the nature of the solvent should influence the ion-molecule chemistry.

Further evidence that neutral excited state homolysis cannot be important is obtained by examining the H_2 and HD yields. The hydrogen yield following photolysis of various aromatic hydrocarbons in cyclohexane is 20-40% lower than the H_2 yield following photolysis of cyclohexane alone—opposite to the trend predicted from the homolysis mechanism.

The H_2 production in cyclohexane is presumed to involve both neutral state homolysis and the loss of molecular hydrogen from the $c\text{-}C_6H_{12}^{+}\bullet$ radical cation to yield the olefin radical cation. Even though there is considerably more light absorption by the solute molecule, one does not completely eliminate solvent photolysis. Solvent-derived products, such as cyclohexene and bicyclohexyl, are observed with or without an aromatic substrate present. Cyclohexene is always the more abundant product, but the bicyclohexyl yield is considerably increased (Table 2) when an aromatic solute is present. Previous workers have shown that if only the cyclohexyl radical were involved, then one would obtain a 1:1 ratio of cyclohexene to bicyclohexyl.

Table 1. Product and isotope distributions after photolysis of perdeuterated polycyclic aromatic hydrocarbons in various solvents at 248 nm[a]

substrate/solvent	parent ion	isotopic ion	Δ%[b]	% yield of cyclohexyl radicals[c]	% substrate consumed
naphthalene/cyclohexane	$C_{10}H_8$	$C_{10}H_7D$	0.1	10.9	43
naphthalene/cyclohexane(d12)	$C_{10}H_8$	$C_{10}H_7D$	8.0	11.0	41
naphthalene(d8)/cyclohexane	$C_{10}D_8$	$C_{10}HD_7$	7.9	11.4	44
naphthalene(d8)/cyclohexane[d]	$C_{10}D_8$	$C_{10}HD_7$	2.2	3.2	26
naphthalene(d8)/isopropanol	$C_{10}D_8$	$C_{10}HD_7$	8.6	-	-
p-terphenyl(d14)/cyclohexane	$C_{18}D_{14}$	$C_{18}HD_{13}$	4.7	-	-

[a]The samples consisted of 3.0 ml solution in a 1-cm path-length cell, saturated with SF_6. The concentration of each substrate was as follows: naphthalene, 4×10^{-4} M; p-terphenyl, 2×10^{-4} M.
[b]Δ% was determined by subtracting the relative abundance of the isotopic ion before irradiation from the relative abundance of the isotopic ion after irradiation, taking into account the contribution of ^{13}C isotopes.
[c]Determined by multiplying the yield of bicyclohexyl by four, and then dividing by the initial concentration of aromatic substrate (assuming bicyclohexyl yield is representative of the overall radical yield).
[d]Photolysis carried out at 308 nm.

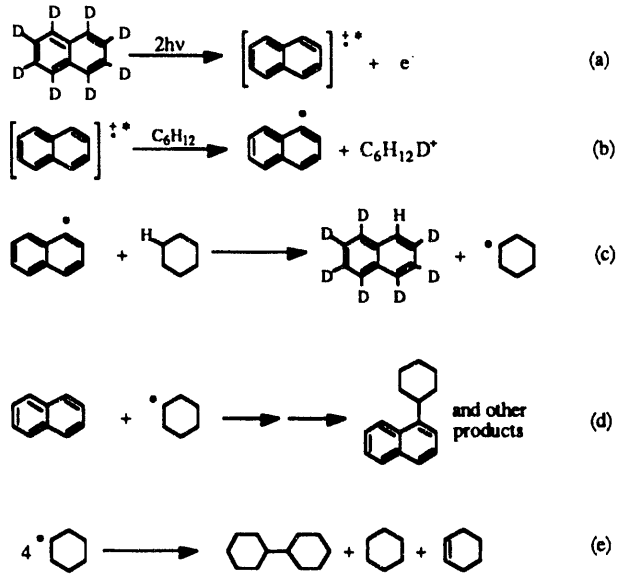

Scheme 3. Aryl and cyclohexyl radical formation and subsequent reactions with isotopically labeled naphthalene.

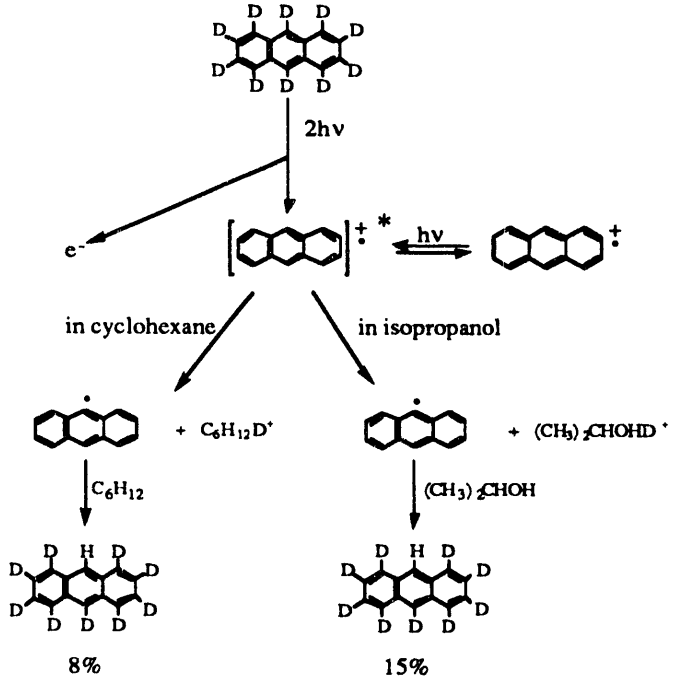

Scheme 4. Aryl radical formation during flash photolysis (248 nm) of d_{10}-anthracene in cyclohexane or isopropanol.

If homolysis were the only pathway, photolysis of a perdeuterated substrate would result in the formation of a substantial amount of HD. For photolysis of d_{10}-anthracene in cyclohexane, 1.6 mM bicyclohexyl and 7.0 mM cyclohexene were formed. Assuming one product molecule formed per dihydrogen molecule, the maximum relative yield of HD in the H_2 + HD yield would be about 37%. Mass spectral data indicate a much lower value, merely 1.5%.

The effect of SF_6 on product formation is also indicative of an ion reaction, not excited state homolysis. SF_6 increases the yield of radical-derived products. Because electron scavenging reduces ion-electron recombination, it increases the yield of ion-molecule reactions (Table 2). The effect of SF_6 on excited state homolysis would be exactly opposite; one would expect a decrease in the yield because SF_6 quenches the excited state.

Table 2. Relative yields of bicyclohexyl from the photolysis of cyclohexane at 248 nm with and without naphthalene and SF_6.

	bicyclohexyl yield during photolysis of cyclohexane only	bicyclohexyl yields during photolysis of cyclohexane in the presence of naphthalene
no SF_6	5.3	4.3
SF_6	1.0	10.0

The degassed samples consisted of 3.0 ml solution in a 1-cm path-length cell. The naphthalene concentration was 1×10^{-3} M. Product yields are relative to the yield of bicyclohexyl in SF_6-saturated solvent alone (actual yield, ~3×10^{-5} M).

Flash photolysis and DC-conductivity studies. The transient optical absorption spectrum of $AH^{+\bullet}$ can be measured by nanosecond flash photolysis. The electron yield can be measured by conductivity in hydrocarbon solutions or by optical absorption in alcohols (Figure 10).

In hydrocarbons, one observes that the yields of $AH^{+\bullet}$ and e^- diverge with increasing photon energy; the electron yield increases, but less $AH^{+\bullet}$ is formed at higher photon energies. The experiments in alcohol solutions indicate that, at high light intensities, the ratio, $e^-/AH^{+\bullet}$, can be quite large, as illustrated in Figure 11 for anthracene/2-propanol photolysis.

These observations suggest the emergence of a three-photon process at high intensities. In other words, the initial radical ion formed by biphotonic ionization absorbs another photon to form an excited radical ion ($AH \xrightarrow{2h\nu} AH^{\bullet+} \xrightarrow{h\nu} AH^{*\bullet+}$), leading to even more products. Also, the product yields are qualitatively correlated with the larger $e^-_{sol}/AH^{+\bullet}$ ratios at high light intensity.

In conclusion, these studies indicate that multi-photon absorption can induce ion-molecule chemistry in aromatic molecules in hydrocarbon and alcohol solutions. It is not yet clear to what extent two- or three-photon processes are involved, and what the excited states of the aromatic radical cation AH^{*+} are. What is clear is that a common pathway of chemistry opens with intense UV light for a variety of aromatic compounds in very different solvents, and that this pathway must involve ion-molecule reactions of an excited AH^{*+} aromatic radical cation.

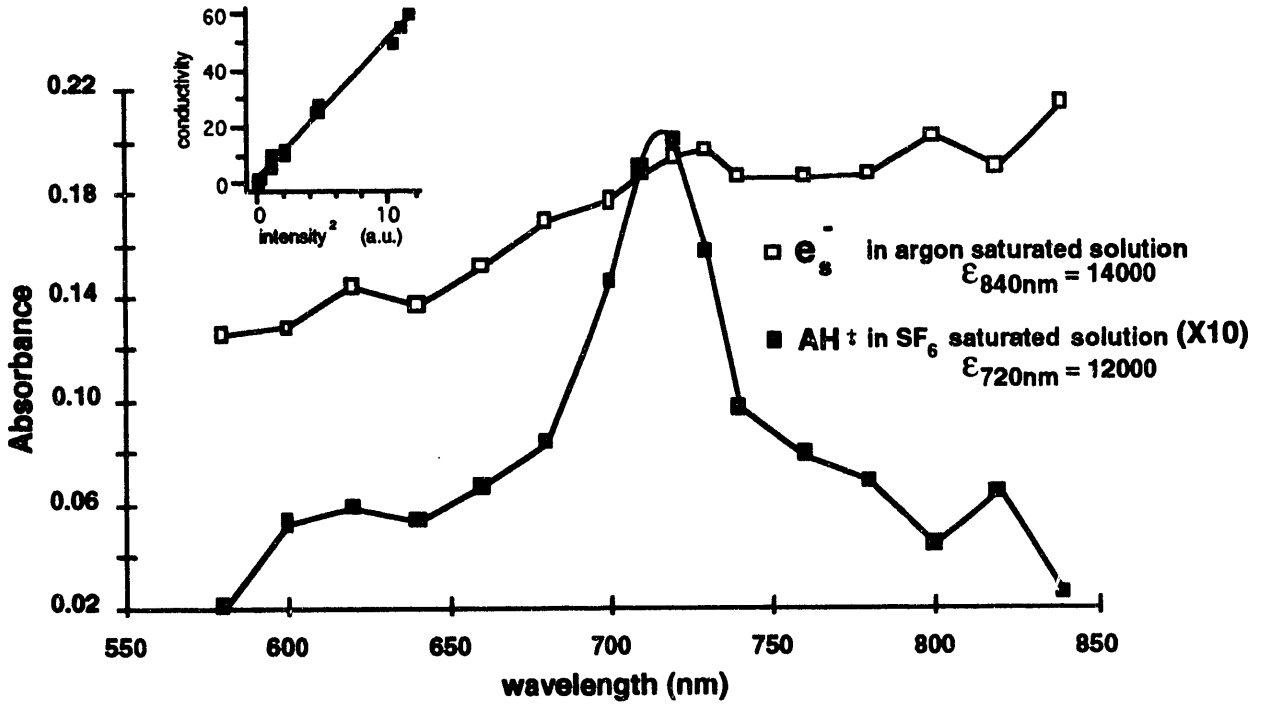

Figure 10. Spectrum of solvated electrons and anthracene radical cations observed at 50 ns after 248-nm laser flash photolysis of 5×10^{-5} M anthracene in 2-propanol.

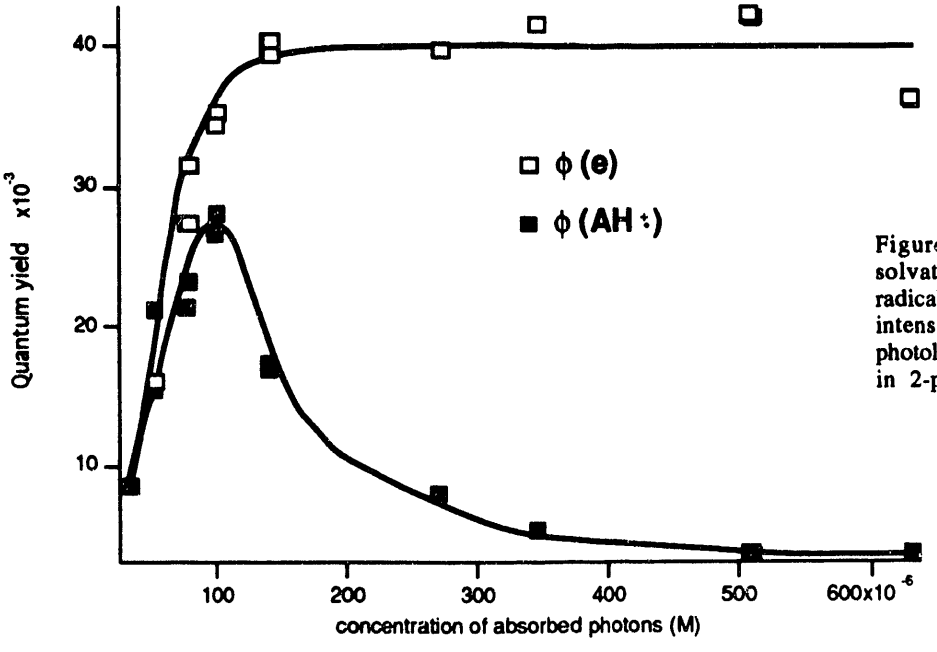

Figure 11. Quantum yields of solvated electron and anthracene radical cation as a function of laser intensity during 248-nm laser flash photolysis of 5×10^{-5} M anthracene in 2-propanol.

4. Ions and Excited States in Radiolysis and Photolysis

M. C. Sauer, Jr., C. D. Jonah, A.-D. Liu, D. M. Loffredo, A. D. Trifunac

We have carried out experiments on the decay of ions and the formation of excited states in solutions of aromatic molecules in alkane liquids. One objective was to determine the ratio of excited states formed to solute anions recombined; the extent to which this is less than unity tells us the extent of transformation of solvent cations to species that cannot yield excited solutes. Another objective was to determine the ratio of solute triplet states to solute excited singlet states; this gives us a measure of the cross-recombination occurring in multiple-ion-pair spurs and therefore allows a comparison with predictions of the distribution of spur sizes made on the basis of other experimental and theoretical information. Our experiments provide the first determination of the triplet-to-singlet ratio as a function of time.

a. Ion-Recombination in Spurs

The nonhomogeneous kinetics of ion-recombination resulting from the radiolytic ionization of an alkane liquid pertain mainly to the time regime of 0-100 ns. The recombinations occur in single ion pairs and in multiple-ion-pair "spurs". For a single ion pair, the recombination is called "geminate", and will produce a singlet state product (whether electron or positive-ion scavenging has occurred or not) unless spin dephasing has occurred. Spin dephasing/evolution is generally expected to occur after tens of ns. For a multiple-ion-pair spur, cross-recombination events are expected to produce triplet state products 75% of the time. Measurement of the triplet yield in the first 10-20 ns is therefore of prime importance to assess the extent of cross recombinations.

Experiments to address this question have been completed with isooctane, cyclohexane, and n-hexane solutions containing 0.1 M naphthalene or biphenyl. The high concentration is advantageous for three reasons. First, the electrons, positive ions, and solvent excited states are captured by the solute in subnanosecond times, and the rates of triplet and singlet formation from one to tens of nanoseconds represent those from the spur recombinations. Second, more recombinations take place at early times, before spin dephasing is significant; and third, the excited state yields are larger, resulting in a better signal-to-noise ratio.

We measured the time profile of the optical absorbance of triplet naphthalene (^{3}N) following a 30-ps pulse, and converted the results to G values (number per 100 eV absorbed energy) by using the known absorptivity of ^{3}N. The time profile of the fluorescence from the first excited singlet state of biphenyl (^{1}BP) was measured and converted to a ^{1}BP formation curve by a simple mathematical procedure using the known fluorescence lifetime of ^{1}BP. This was converted to G(^{1}BP) on the basis of our previous measurements of G values of aromatic singlets. The derivatives of these G vs. time profiles were then calculated and plotted vs. time. The results are illustrated for isooctane solutions in Figures 12 and 13.

Values of d/dt taken from Figures 12 and 13, and from similar plots for cyclohexane and n-hexane, were used to calculate the fraction of triplet, $f_{triplet}(t)$ from 1-70 ns. $f_{triplet}(t)$ is the ratio of the rate of triplet formation at time t to the sum of the rates for singlet and triplet. It represents the probability of triplet formation in the ion recombination occurring at time t. The results are shown in Figure 14.

There are three main features. (1) The formation of the triplet state and formation of the excited singlet state is equally probable when ion recombination occurs in the time regime 1-70 ns, with the following caveat: the values of $f_{triplet}(t)$ depend on the calibration factors used for both the singlet and triplet G-value scales; hence, the vertical scale could have an error of as much as 10-20%. (2) Within the experimental error, there is no tendency of $f_{triplet}(t)$ to increase with time. This finding indicates the absence of an appreciable effect of spin dephasing in the geminate pairs over the time regime 1-70 ns. (3) The values of $f_{triplet}$ for isooctane seem to be significantly higher than for cyclohexane and n-hexane. This result suggests that the known greater average separation between the geminate partners in isooctane is responsible, that is, that greater separation favors cross-recombination in multiple-ion-pair spurs.

Most of the values of $f_{triplet}(t)$ are in the range of 0.5 ± 0.1. This value can be compared with the results from cloud chamber measurements and theoretical calculations of the number of ion pairs per spur, as shown in Table 3.

In Table 3, it is assumed that N_s, and hence, $f_{triplet}$, is independent of t. The last two columns give the $f_{triplet}$ values for spurs of various sizes

(numbers of ion pairs) for two different theories (Magee and Brocklehurst). Column 2 gives the fraction of the total ion pairs that are created (by a high-energy electron) in spurs of the size indicated in column 1. The sum of the numbers in the last two columns is the resultant $f_{triplet}$. Our experimental values, 0.5 ± 0.1, are somewhat higher than the values of 0.39 and 0.45 from Table 3, but are within experimental error.

In view of the possibility that an error in the relative scaling of the ^3N and ^1BP G values could have a significant effect on the value of $f_{triplet}$, another method has been used to derive the value of $f_{triplet}$ from experimental observations. The formation of ^3N has been measured with subnanosecond time resolution (approximately 0.3 ns) from 0.1-1000 ns, and the results have been fitted to a mechanism that takes into account the known reactions, with $f_{triplet}$ as a

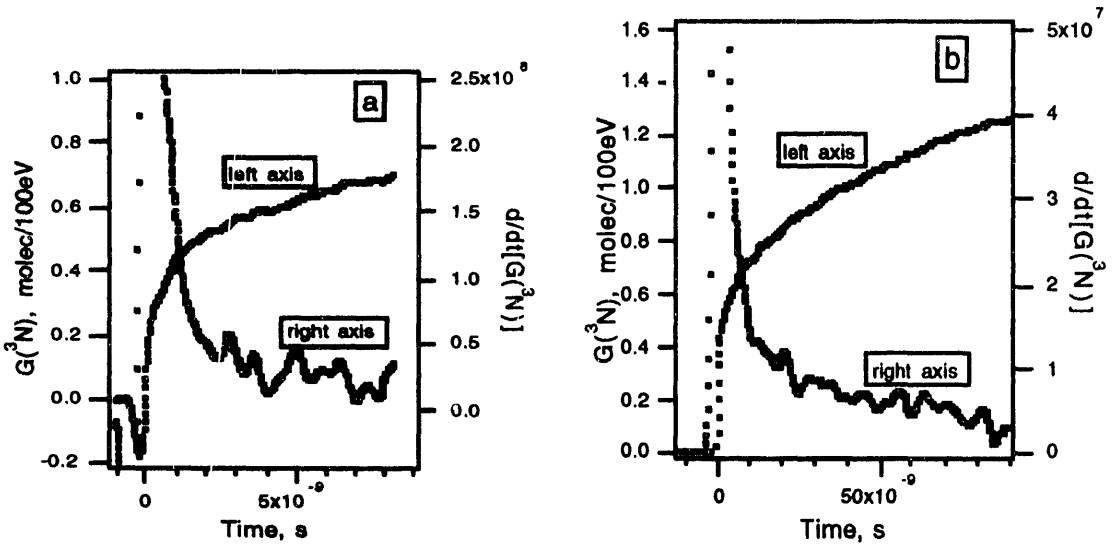

Figure 12. $G(^3N)$ and d/dt of $G(^3N)$ vs. time for 0.1 M naphthalene in isooctane. Electron pulse: 30 ps, 5.4 krad. (a) 0-9 ns; (b) 0-85 ns.

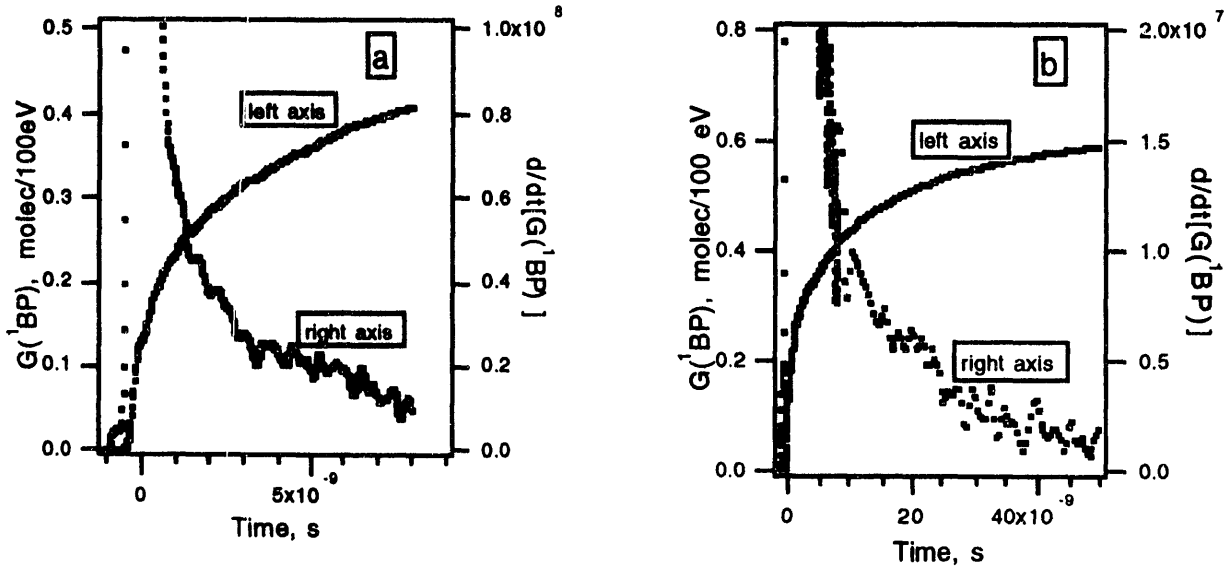

Figure 13. $G(^1BP)$ and d/dt of $G(^1BP)$ vs. time for 0.1 M biphenyl in isooctane. Electron pulse: 30 ps, 4.0 krad. (a) 0-8 ns; (b) 0-50 ns.

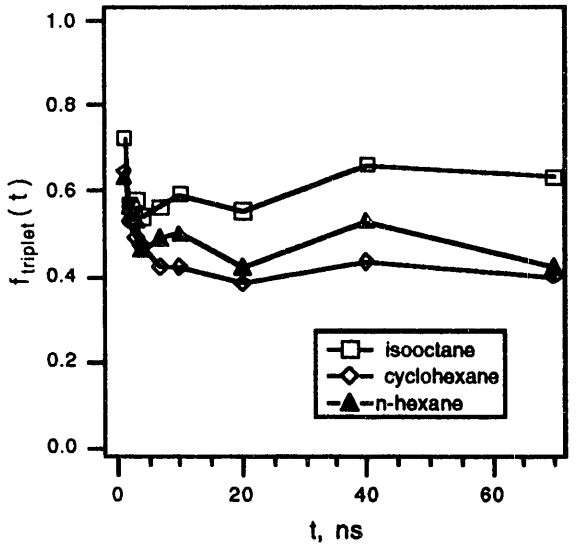

Figure 14. Fraction of excited states formed at time t that are triplet; 0.1 M solutions of naphthalene or biphenyl in the indicated solvents.

fitted parameter. The experimental $G(BP^-)$ vs. time results are used to specify the rate of ion recombination. The long lifetime of the first excited singlet state of naphthalene (95 ns) makes this solute ideal for this analysis; the triplet observed in the first few tens of nanoseconds must originate mainly from ion recombination (rather than from intersystem-crossing from the singlet). The results for 0.1 M naphthalene in isooctane are shown in Figure 15. The value of $f_{triplet}$ derived from this method is 0.52 ± 0.05, which is in good agreement with the values from the derivative analysis. Note that the quality of the fit was not improved by allowing $f_{triplet}$ to vary with time, also in agreement with the derivative analysis.

The analysis of $f_{triplet}$ in radiolysis that we have presented here is the most complete and decisive to date, and is the first to examine specifically the time dependence of $f_{triplet}$ The values of $f_{triplet}$ are consistent, within experimental error, with expectations based on analyses of the energy-deposition events in terms of spur-size distribution and cross-recombinations among geminate pairs.

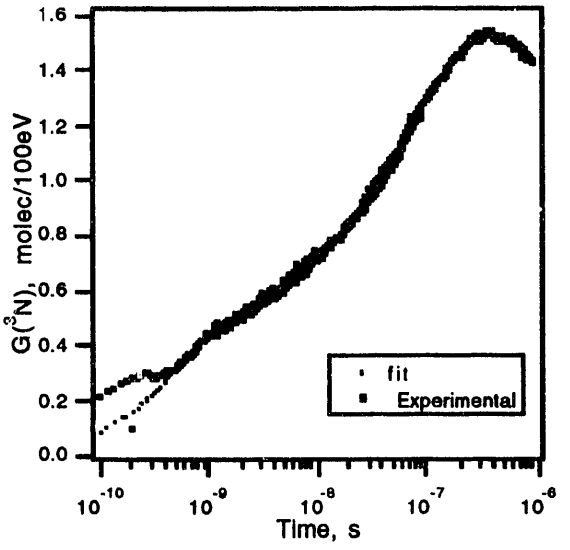

Figure 15. $G(^3N)$ vs. time for 0.1 M naphthalene in isooctane; experimental and calculated results.

b. Anion Decay vs. Excited State Formation

In conjunction with the measurements of G values of solute excited singlet and triplet states described above, we also measured the G value of the biphenyl anion, BP^-, as a function of time for 0.1 M biphenyl in isooctane, cyclohexane, and n-hexane. Values of d/dt of $G(BP^-)$ were determined in the same

Table 3. Predicted values of $f_{triplet}$

n, ion pairs per spur	fraction (F) of ion pairs (Hummel)	singlets per recombin., N_s, (Magee)	singlets per recombin., N_s, (Brocklehurst)	$f_{triplet} = F \times (1 - N_s)$, (Magee)	$f_{triplet} = F \times (1 - N_s)$, (Brocklehurst)
1	0.30	1.000	1.000	0	0
2	0.17	0.500	0.625	0.085	0.064
3	0.10	0.400	0.500	0.060	0.050
4	0.05	0.357	0.437	0.032	0.028
>4	0.38	≅0.29	≅0.33	≅0.27	≅0.25
				sum = 0.45	sum = 0.39

manner as described for ^3N and ^1BP. Comparison of the rate of BP^- decay with total excited state (^3N + ^1BP) formation rate is shown in Figure 16, where f_{ex} is the ratio of the sum of the rates of excited state formation divided by the rate of BP^- decay.

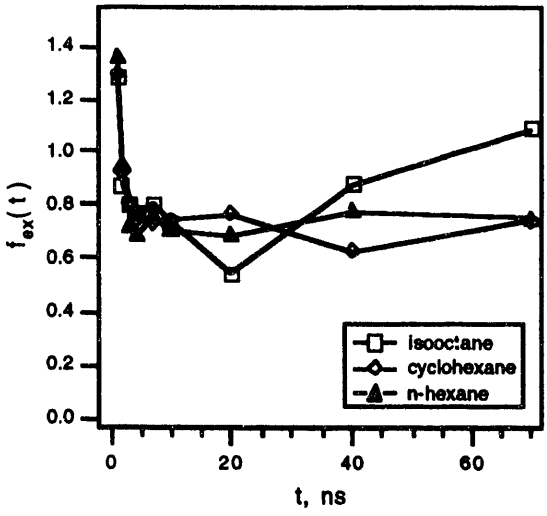

Figure 16. The ratio of excited state formation to BP^- decay from 1-70 ns.

There are rather large variations in f_{ex} with time. The very high values at 1 ns could be the result of experimental errors, or they could indicate the transformation of solvent radical cations, prior to scavenging by the solute, to species unable to provide excited solute. The variations at later times, and differences between solvents, are most likely due to experimental error. The fact that most f_{ex} values are in the range of 0.7-0.9 means that 70-90% of the solute radical anions recombining in the 1-70 ns regime yield excited states. This finding means that 70-90% of the radical cations that recombine in the specified time regime cannot have been converted to a form that is unable to yield excited solute. Thus, at 0.1 M solute, only a small fraction of the solvent radical cations have undergone ion-molecule reaction with the solvent. This is not surprising, because at 0.1 M solute, transfer of charge from the solvent radical cation to the solute should be very rapid ($t_{1/2}$ < 0.7 ns). Therefore, ion-molecule reactions of the solvent radical cation with the solvent to form cations unable to yield excited states, which are about an order of magnitude slower, do not consume a large fraction of the solvent radical cations.

c. Formation of Aromatic Radical Cations in Alcoholic Solutions; the SF_5· Radical as an Oxidizing Species

We have determined that aromatic radical cations are formed in large yields in the pulse radiolysis and laser flash photolysis of SF_6-saturated alcoholic solutions of aromatic molecules. Intense, long-lived absorptions are observed when SF_6 is present. The rate of formation of the absorption is proportional to the concentration of the aromatic molecule. As an example, Figure 17 shows the spectra, at three times after the laser pulse, observed for SF_6-saturated 5 × 10^{-4} M anthracene in methanol using 308-nm laser flash photolysis. The 720-nm absorption corresponds to the known absorption maximum for the anthracene radical cation. The spectrum labeled 20 ns (essentially determined during the laser pulse) consists of the first excited singlet state of anthracene (600 nm), the anthracene radical cation (720 nm), and a broad underlying absorption due to the steady-state concentration of solvated electrons.

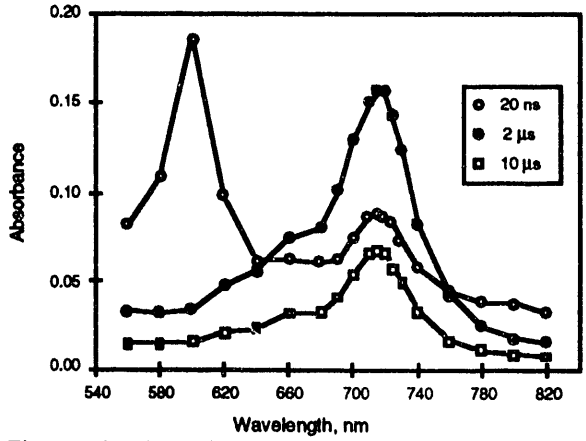

Figure 17. Absorption spectra for 308-nm laser flash-photolysis of SF_6-saturated 5 × 10^{-4} M anthracene in methanol.

The slow formation (Figure 18) occurring over about 800 ns was analyzed; the pseudo-first-order rate constants obtained were linear with [anthracene], yielding a rate constant of 8 × 10^9 M^{-1} s^{-1} for formation of the anthracene radical cation.

The absorption of the anthracene radical cation in the case of pulse radiolysis of SF_6-saturated 5 × 10^{-4} M anthracene in 2-propanol is shown in Figures 19 and 20.

In pulse radiolysis (Figure 20), the radical cation is formed only by the "slow" process, which is

thought to be the reaction of SF_5·, which results from the dissociative capture of a solvated electron by SF_6, with the aromatic molecule.

The G values and rate constants in Table 4 indicate that the efficiency of oxidation of the aromatic molecules by SF_5· depends strongly on their ionization potentials and the solvent polarity. SF_5· appears to react with the aromatic molecules via two different pathways, one of which forms the aromatic radical cation and the other of which leads to unidentified products.

Further study will be needed to reveal key details of primary and secondary processes initiated by the UV irradiation or ionizing radiation in the condensed phase. The formation of long-lived aromatic radical cations in alcohols by laser flash photolysis and pulse radiolysis provides a convenient method to generate the aromatic radical cations and enables the study of their properties and reactions in the liquid phase at room temperature. A systematic investigation of the formation of aromatic radical cations by laser flash photolysis and pulse radiolysis with other important aromatic molecules and different electron scavengers in different solvents will make it possible to delineate the energy dependence of these reactions and to assign the role of the solvent in the reactions.

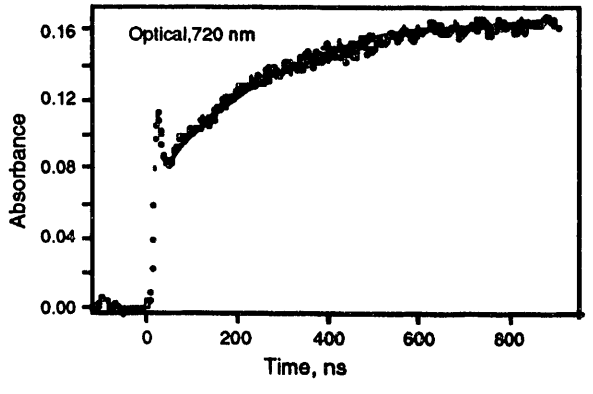

Figure 18. Absorption at 720 nm vs. time for 308-nm laser flash photolysis of SF_6-saturated 5 × 10^{-4} M anthracene in methanol.

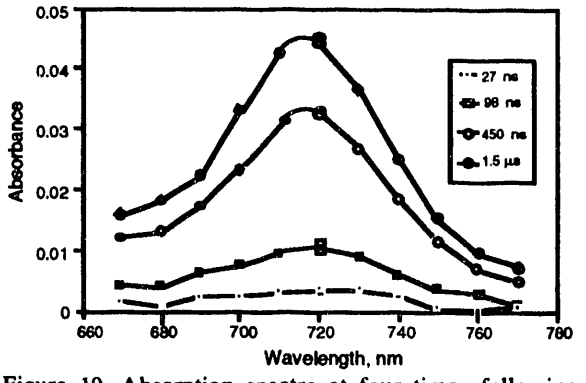

Figure 19. Absorption spectra at four times following an electron pulse (1.8 krad dose per pulse) in SF_6-saturated 5 × 10^{-4} M anthracene in 2-propanol.

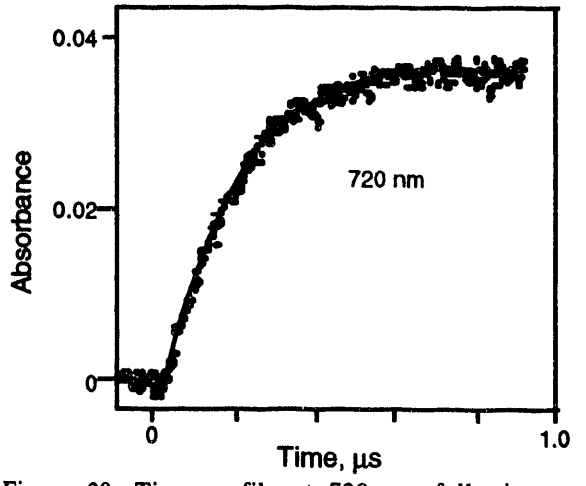

Figure 20. Time profile at 720 nm following an electron pulse (1.8 krad dose per pulse) in SF_6-saturated 5 × 10^{-4} M anthracene in 2-propanol.

Table 4. G-values and rate constants derived from the formation of aromatic radical cations in the pulse radiolysis of SF_6-saturated 2-propanol and methanol solutions.[a]

solute	IP (eV)	λ_{max} (nm)	ε (M^{-1} cm^{-1})	G (per 100 eV) 2-propanol	G (per 100 eV) methanol	10^{-9} k (M^{-1} s^{-1}) 2-propanol	10^{-9} k (M^{-1} s^{-1}) methanol
perylene	7.0	540	3.5×10^4	1.74	—	4	—
anthracene	7.5	720	1.2×10^4	1.72	—	8	8[c]
hexamethylbenzene	7.9	500	2.33×10^3	0.56	4.26	2	1.7
naphthalene	8.1	690	2.70×10^3	<0.1	0.44[b]	—	—

[a]IP is the gas-phase ionization potential of the aromatic molecule from the literature. λ_{max} is the absorption maximum of the solute radical cations. ε is the molar absorptivity of the solute radical cations from the literature. [b]This value was obtained at 0.01 M naphthalene; G is approximately proportional to [N]. [c]Measured by laser flash photolysis.

B. The Role of Solvent in Chemical Reactivity

A. D. Trifunac, D. M. Bartels, C. D. Jonah, Y. Lin, K. H. Schmidt, P. Han, C. Romero, E. Roduner

1. Reaction of H Atoms with Benzene in Water

D. M. Bartels, E. Roduner

Solvent effects on chemical reaction rates have been investigated in detail for many years and general trends are understood for many reaction types in terms of dielectricity and ionic strength of the medium. The primary interest is the extent to which a given solvent, depending on its dielectric properties and molecular structure, might enhance or retard particular types of reaction. The transition state theory of reaction rates is generally invoked to understand solvent effects, in terms of "stabilization" or "destabilization" of reactants or products or a postulated transition state. A fundamental and largely untested assumption is made in the application of transition state theory to reactions in solution. This is the assumption that equilibrium thermodynamics applies to the transition state as well as to the reactants and products. In view of the highly transient nature of the transition state configuration, it is questionable that a solvent would have time to fully equilibrate about the transition state. In this case, correlation of reaction rates with equilibrium solvent properties may be based on a shaky theoretical foundation.

To investigate this issue, we undertook a study of the addition reaction of hydrogen isotopes to benzene in aqueous solution. Reliable data for this reaction in the gas phase are available, and a study of the analogous light muonium atom (μ^+...e^-) reaction with benzene in several solvents has also been published. In the gas phase, the reaction of H with benzene occurs by addition, with a negligible amount of abstraction at temperatures below 1000 K. The reaction is one of the few simple hydrogen additions that are significantly activated. Addition of the light muonium atom (mass one-ninth of H) has a rate considerably enhanced by tunneling through the barrier, as evidenced by a much lower activation energy and lower frequency factor. Our invention of the EPR-based free induction decay attenuation method makes feasible a study of the the H- and D-atom reactions with benzene simultaneously in the same aqueous solvent environment. The results allow a test of the transition state theory assumptions for this system. As we describe below, the results suggest that reactions of H and D may occur with nearly complete hydration of the transition state, but the reaction of Mu must occur too quickly for the water to equilibrate.

ESR measurement of the H-atom reaction rate by the FID attenuation method was chosen because of its simplicity, and the ability to measure H and D reactions simultaneously. Figure 21 shows a representative example of a scavenging plot of FID attenuation rate vs. benzene concentration. The slope of the plot gives directly the H (or D) atom scavenging rate. The data were obtained with a mixture of 10% H_2O/90% D_2O, so that H and D atoms were both observed in the same experiment. The different slopes show clearly that there is an isotope effect that favors the reaction of H over that of D. Furthermore, there is a small but significant difference in the intercept of the two lines. Inasmuch as H and D data points were obtained alternatingly with the identical solution, the 8.6% larger value of the intercept shows that H is slightly more efficient in second-order spin exchange processes. This fact indicates that diffusion is slightly faster for H than for D.

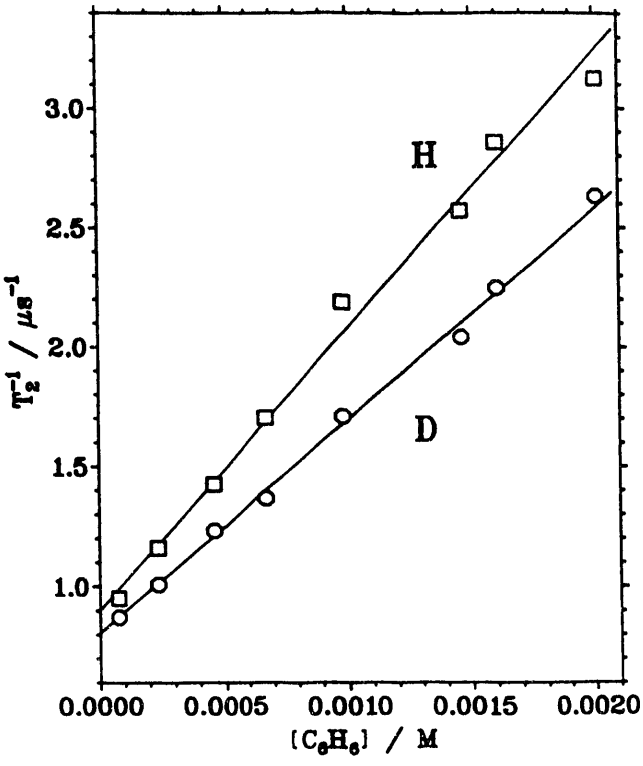

Figure 21. Inverse relaxation time as a function of benzene concentration for H and D in a mixture of 10% H_2O/90% D_2O at 297.5 K.

The temperature dependence of k_H is displayed in an Arrhenius plot in Figure 22 (open symbols). There is no systematic deviation between the points obtained in neutral solution with t-butanol scavenger (squares) and those measured in acidic solution with methanol scavenging (crossed squares). The points for H in the H_2O/D_2O mixture lie on the same line, but those representing k_D are clearly lower. There is a slight curvature, but the average Arrhenius parameters are E_a = 19.1 kJ/mole and log (A/sec) = 12.34 (full line in Figure 22). The activation energy is within error the same in aqueous solution as in the gas phase. The enhanced rate constant in solution is reflected almost entirely by the larger frequency factor, A(aq)/A(g) = 54.

Transition state theory gives the rate constant for bimolecular reactions as equation 10:

$$k = q \cdot T \cdot \exp\left(\frac{\Delta S^{\neq}}{R}\right) \cdot \exp\left(\frac{-\Delta H^{\neq}}{RT}\right), \qquad (10)$$

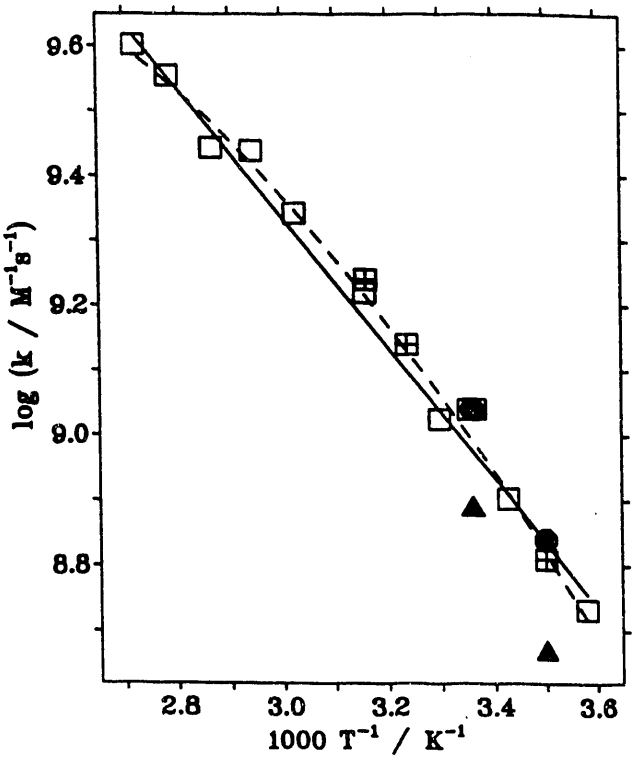

Figure 22. Arrhenius plot of the rate constant for the reaction with benzene. H in H_2O (open squares, crossed where methanol was used to scavenge hydroxyl radicals), H (filled circles), and D (filled triangles) in a mixture of 10% H_2O/90% D_2O. Normal Arrhenius (full curve), modified with heat capacity term (broken curve, see text).

where q•T includes universal constants and has the units of k. This may lead to a curved Arrhenius plot, in particular when activation entropy and enthalpy are temperature dependent. Assuming a constant heat capacity difference between reactants and transition state and using standard thermodynamics, we obtain equation 11,

$$\ln k(T) = \ln(q \cdot T_o) + \frac{\Delta S_o^{\neq}}{R} + \left(\frac{\Delta C_p^{\neq}}{R} + 1\right)\ln\left(\frac{T}{T_o}\right) - \frac{\Delta H_o^{\neq} + \Delta C_p^{\neq}(T - T_o)}{RT}, \qquad (11)$$

where $\ln(q \cdot T) + \frac{\Delta S_o^{\neq}}{R}$ is the natural logarithm of the Arrhenius frequency factor at T_o. The broken line in Figure 22, a fit of the experimental data to equation 11, is clearly a better representation of the experimental points than the straight line.

For interpretation of the solvent effects on the reaction rate we compare the reaction in the gas phase with that in solution as in Scheme 5:

$$\begin{array}{lccccc} \text{Gas:} & H & + & C_6H_6 & \xrightarrow{k_H(g)} & [C_6H_6 \cdots H]^{\neq} \\ & \downarrow \Delta G^{H}_{solv} & & \downarrow \Delta G^{C_6H_6}_{solv} & & \downarrow \Delta G^{\neq}_{solv} \\ \text{Solution:} & H & + & C_6H_6 & \xrightarrow{k_H(aq)} & [C_6H_6 \cdots H]^{\neq} \end{array}$$

Scheme 5

Based on transition state theory, equation 10, the enhancement due to solvation is given by equation 12:

$$\frac{k(aq)}{k(g)} = \frac{K^{\neq}_{(aq)}}{K^{\neq}_{(g)}} = \exp\left(\frac{-\Delta G^{\neq}_{solv} + \Delta G^{C_6H_6}_{solv} + \Delta G^{H}_{solv}}{RT}\right) \qquad (12)$$

The solubility of benzene in water is well established as a function of temperature, and has been critically reviewed. The solvation properties of the transition state are, of course, not known, but may be estimated by averaging the results for benzene and for 1,4-cyclohexadiene. Previously, the solvation property of the hydrogen atom has been estimated by averaging the free energy of solvation of H_2 and of He. We propose to use the values of H_2 alone for the reason outlined here. The solvation enthalpy is governed largely by dispersion forces and is therefore a strong function of solute polarizability. The polarizability of

H atoms (alpha = 8.7×10^{-31} m^3) is much closer to that of H_2 (7.9×10^{-31} m^3) than to that of He (2×10^{-31} m^3). The entropy of solvation is a large negative number for all noble gas atoms and small molecules (46.7 J/mol•deg for H_2 at 298 K, nearly the same number as for benzene and cyclohexadiene). Assuming that the entropy of solvation is the same for H as for H_2, we conclude that the free energy of solvation of atomic hydrogen is approximated well by that of molecular hydrogen.

The predicted values of k(aq)/k(g) based on equation 12 and the strategy outlined above are compared with experiment (squares) in Figure 23 (solid line). The agreement is striking in that the experimental points fall only about 10% short of the prediction. Also shown (broken curve) is the predicted behavior based on the approximation (found to apply to muonium reactions in previous studies) that the benzene molecule and the transition state are sufficiently similar with respect to solvation so that the corresponding free energies cancel. In that case, the enhancement factor is given solely by the free energy of solvation of the hydrogen atom, equation 13:

$$\frac{k(aq)}{k(g)} \equiv \exp\left(\frac{-\Delta G^{H}_{solv}}{RT}\right) = L^{-1} \qquad (13)$$

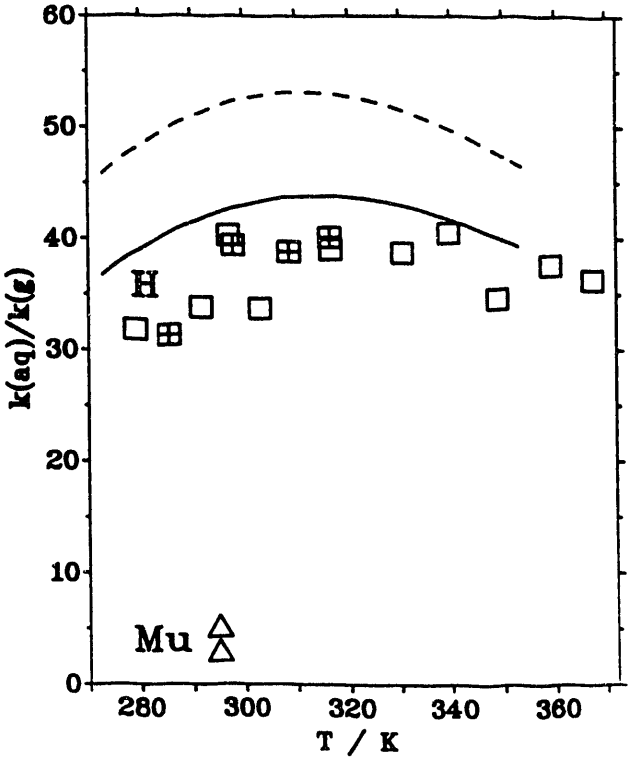

Figure 23. Enhancement factor of the rate constant in aqueous solution over the corresponding gas-phase value. The broken line gives the predicted curve based on ΔG_{hyd} of H_2 alone, equation 13, and the solid curve represents the full equation 12.

Comparison of the two lines in Figure 25 demonstrates that 80% of the enhancement effect can be ascribed to solvation of the H atom. The remaining deviation between the best prediction and the experiment can easily be ascribed to experimental error and the approximations made in estimating the solubility of H and of the transition state. It should be noted, however, that the curve is shifted to much higher values and thus far from our experimental data for k(aq)/k(g) when H solvation is approximated by He instead of by H_2.

The preceding analysis suggests that essentially the full solvent enhancement effect for the reaction of H with benzene in water is explained in terms of equilibrium solubility of reactants and transition state. The same conclusion has been reached previously for the reaction of benzene with muonium in methanol and in hydrocarbon solution where the enhancement was less drastic. This implies that the transition state is also fully equilibrated for the muonium addition in these less polar solvents. However, the muonium reaction in water is different, as indicated by the points in Figure 23. The solvent enhancement is only a factor of four rather than the predicted factor of 40. The question then arises, why is the muonium reaction rate enhanced less than the rate for H and D in aqueous solution?

The negative solvation entropies indicate that both the hydrogen atom and the benzene molecule reside in "clathratelike" hydrophobic cages. The two cages must merge prior to the reaction. In order that advantage can be taken of the full free enthalpy of solvation, there has to be complete relaxation of the solvent around the transition state on the time scale of barrier crossing. Comparison between the experimental and predicted values in Figure 23 indicates that this is the case for H but suggests that it may not be so for the light muonium atom (atomic mass 0.11). Because the addition reaction is exothermic and the transition state early, the effective mass moving along the reaction coordinate will essentially be that of the adding hydrogen isotope. Based on the mass dependence of the imaginary frequency that describes the degree of freedom corresponding to the reaction coordinate, the light Mu atom is expected to move

over or through the barrier about three times faster than H. This motion is effectively a low-frequency vibration that occurs on a time scale similar to the libration of the water molecules. It is thus conceivable that we have a borderline case in water, where relaxation of the cage, involving reorientation of water dipoles, is nearly complete for H but too slow for Mu. Only the high-frequency (electronic) part of the solvent polarizability would then be able to follow Mu through the transition state. Because in water this is only a fraction of the total dielectric response, solvation of the transition state would be incomplete and the assumption of equilibrium between reactants and transition state not appropriate.

2. Mechanism of the $(H)_{aq} \rightleftharpoons (e^-)_{aq}$ Interconversion *D. M. Bartels and P. Han*

The hydrated electron is arguably the most important transient species in the radiolysis of water, and is certainly the most interesting and unusual. In years past, investigations in this group have focused on the dynamics of electron energy loss as the electron becomes trapped and then fully solvated. More recently, we have addressed the equilibrium thermodynamic and transport properties of the fully solvated species, to contrast the prototypical quantum ion with more common classical species. The thermodynamic properties of the hydrated electron were deduced from the highly unusual reaction of H or D with OH^-/OD^-, equation 14, in mixtures of light and heavy water.

$$H\,(D) + OH^-\,(OD^-) \underset{k_{-14}}{\overset{k_{14}}{\rightleftharpoons}} (e^-)_{aq} + H_2O\,(D_2O) \quad (14)$$

A very old, but still unresolved, important question concerns the mechanism of this $(H)_{aq} \rightleftharpoons (e^-)_{aq}$ interconversion. Is the reaction (particularly the back reaction) an electron transfer similar to most other reactions involving $(e^-)_{solv}$, or does the equilibrium involve a proton transfer? If it involves proton transfer, ideas about the mechanism of other hydrated electron reactions may need to be modified. Our goal in the further investigation of equilibrium 14 has been to resolve this question.

In Figure 24 we display new results for the H + OH^- reaction in light water that were obtained with improved methodology and equipment. Superimposed is the least-squares Arrhenius fit obtained in our *previous* work. Clearly, the average result has not changed significantly, but there is a significant improvement in the precision. Least-squares analysis of the new FID attenuation data gives $A = 1.32 \pm 0.17 \times 10^{14}\ M^{-1}\ sec^{-1}$, and $E_a = 38.36 \pm 0.32$ kJ/mole.

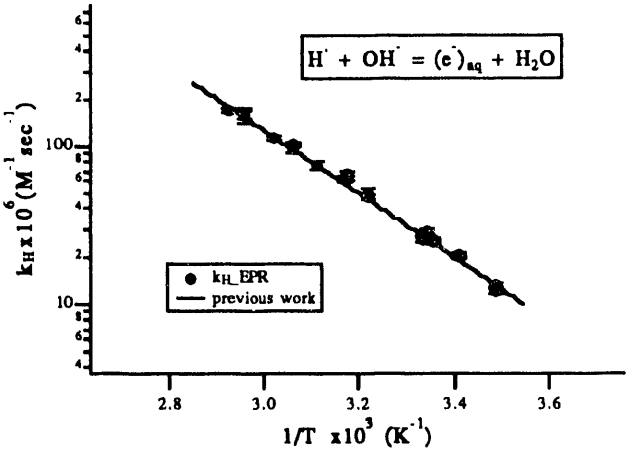

Figure 24. Arrhenius plot for reaction 14 (light water), as measured by the FID attenuation method. The solid line is the least-squares result reported in previous work.

In a recent publication dealing with the hydrated electron thermodynamics, Schwarz raised the possibility that the FID attenuation method may overestimate the rate of reaction 14 if there is also a "base-catalyzed" chemical exchange process occurring. That is to say, H atoms may combine with OH^- to form an intermediate H_2O^-, which dissociates rather than proceeding to the $(e^-)_{aq}$ product. If the "other" proton can emerge from the intermediate to reform the H atom, the proton-exchange event would be indistinguishable from a forward reaction event, so far as FID attenuation is concerned. To examine this possibility, we performed optical transient absorption experiments to measure the rise of $(e^-)_{aq}$ absorption due to reaction 14.

Figure 25 displays a sample of the data for a 0.0467 M NaOH solution at 49.6 °C. The absorption increase seen in the first microsecond(s) of Figure 25 is the signal of interest. The second-order decay of the signal was slow (half-life at least 10 times longer than $1/k_1[OH^-]$), but not negligible on the timescale of reaction 14. We approximate the important kinetic processes as in Scheme 6.

$$(e^-)_{aq} \xrightarrow{kd} \text{products}$$

$$(H)_{aq} \xrightarrow{kd} \text{products}$$

$$(H)_{aq} \xrightarrow{kg} (e^-)_{aq}$$

Scheme 6

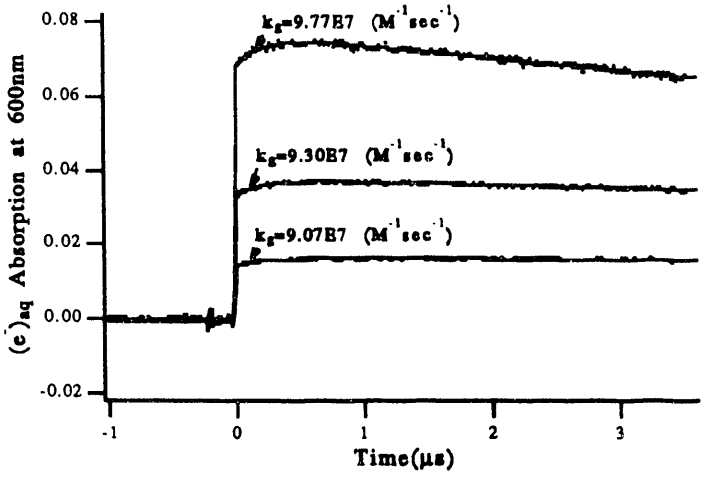

Figure 25. Hydrated electron absorption following pulse radiolysis of 0.01 M Na_2SO_3, 0.046 M NaOH solution at 49.6 °C in triply distilled heavy water. Three different radiolysis doses of ca. 400, 200, and 100 rads to the same solution are shown.

The initial slow rise and roughly the first one-quarter to one-third of the subsequent decay were fit to the corresponding first-order growth/first-order decay function, equation 15,

$$A(t) = A_0 [(C+1) \exp(-k_d t) - C \exp(-k_g t)]$$

$$C = f_H k_d/(k_d + k_g) , \qquad (15)$$

where k_g is the rate of growth, k_d is the rate of decay, f_H is the ratio of yields $G(H)/[G(H) + G(e^-_{aq})]$ immediately after the pulse, and A_0 is the initial absorption. As indicated in Figure 25, the values of k_g extracted from this analysis proved to be slightly dose-dependent, and 5-15% larger than the k_{12} rate constants derived in the EPR experiments. The values of k_g were plotted vs. A_0, and the (zero dose) intercept of the plot was taken for the "best" experimental estimate of k_{12}.

Results of the optical absorption experiment for light water are plotted in Figure 26 together with the least-squares result of the EPR experiments. The good agreement of the two methods makes it clear that a correct result has been obtained, and *no chemical-exchange process contributes to the FID decay.* This conclusion is significant in the following discussion of the reaction mechanism.

EPR and optical experiments were carried out in heavy water, and the combined results are plotted in Figure 27. The FID attenuation experiment in heavy water was far more difficult because of the roughly four times smaller initial CIDEP signal of D atoms in D_2O. This required larger radiolysis pulses and much longer signal averaging to achieve equivalent results. On the other hand, the optical experiment was no more difficult in heavy water. As is obvious from Figure 27, both methods agree to within their signal-to-noise limitations. The global least-squares fit gives $A = 1.19 \pm 0.22 \times 10^{14}$ M^{-1} sec^{-1}, and $E_a = 38.16 \pm 0.47$ kJ/mole for the $D + OD^-$ reaction. The global least-squares result for the *light water* $H + OH^-$ reaction is also superimposed as a solid line in Figure 27. It is clear from this comparison that

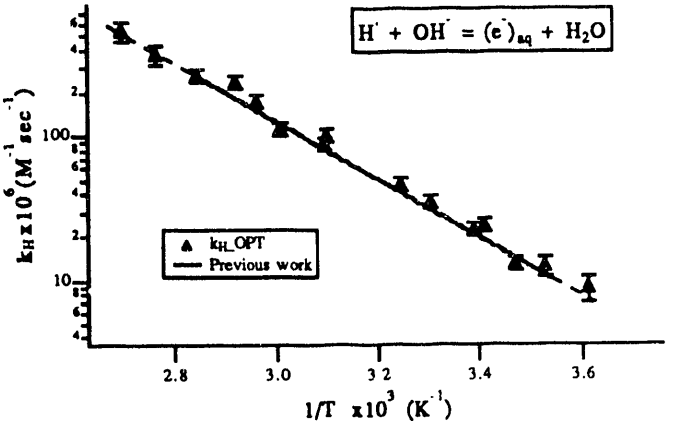

Figure 26. Arrhenius plot for reaction 14 (light water), as determined optically by the rise of $(e^-)_{aq}$ absorption. The solid line is the least-squares result obtained by the FID attenuation method.

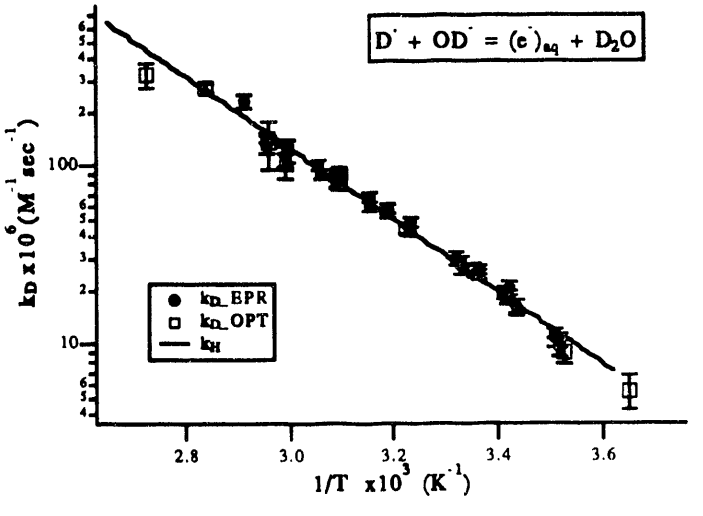

Figure 27. Arrhenius plot for reaction 14 (heavy water). Both FID attenuation and optical experiments are indicated. The solid line is the least-squares result obtained in the *light water* reaction, for purposes of comparison.

there is very little H/D isotope effect on the rate of reaction 14, and within the precision of our measurements, we are unable to clearly define any differences in activation energy and pre-exponential factors. This result contrasts with the order-of-magnitude isotope effect favoring H_2O over D_2O in reaction -14.

With these experimental results in hand, we proceed now to consideration of the reaction mechanism. The encounter of the H atom and hydroxide ion can most easily be envisioned in terms of hydroxide diffusion by proton transfer to a hydrophobic H-atom cavity. The proton-transfer diffusion mechanism will bring the hydroxide into a configuration where the central oxygen and its three strong H bonds form a side of the H-atom cavity. At this point, a sufficiently high-energy collision of the H atom and the oxygen of the hydroxide ion, together with appropriate solvent rearrangement, can form a water molecule and liberate an electron.

The question we wish to address is how this interconversion of $(H)_{aq}$ and $(e^-)_{aq}$ is accomplished, or in other words, what is the nature of the transition state in equilibrium 14? The simplest postulate considers a discrete, H_2O^-, intermediate as shown in equation 16.

$$(H)_{aq} + (OH^-)_{aq} \rightleftharpoons (H_2O^-)_{aq}^{\dagger} \rightleftharpoons H_2O + (e^-)_{aq} \quad (16)$$

Starting from the left side of the equilibrium, one envisions a H atom in a hydrophobic cavity, with the OH^- ion strongly hydrated and incorporated into the hydrogen-bond network. The encounter occurs when the OH^- diffuses to become part of the wall around the H atom. One postulates that the H atom adds to the OH^- ion, forming a transient H_2O^- ion, which then ionizes to give H_2O and an electron that becomes solvated. Starting from the right side of the equilibrium, the electron must somehow become localized on a single H_2O molecule, giving the H_2O^-, which then fragments to give the H and OH^- product.

The simple picture can be rejected based on the results obtained in this study. Any transition state or intermediate that suggests an equivalence of protons, e.g., the $(H_2O^-)^{\dagger}$ formulation, is incompatible with the observation that the overall forward rate (measured optically) is exactly equal to the (EPR) rate of FID attenuation. Modern theories of reaction rates in solution emphasize the diffusive quality of reactive trajectories near the transition-state barrier. The reactants may often cross over the free-energy barrier and then cross back again without ever reaching the final product state. If the transition state in reaction 14 were symmetric or near-symmetric with respect to the two protons, then an exchange of protons between the H atom and the OH^- ion should often occur in those encounters that fail to proceed to product. The FID attenuation rate would be the sum of the forward reaction rate and one-half the proton exchange rate. The experiments indicate that no "base-catalyzed" proton exchange occurs. Therefore, the transition state should more properly be formulated $(H{\bullet\bullet\bullet}OH)^-$, with the location of the "excess" charge still to be specified.

In fact, the transition state of equilibrium 14 should be inherently asymmetric by virtue of the solvent cavity or void occupied by either the H atom (left side of equilibrium 14) or by the electron (right side). In terms of the picture we have described for the encounter of H and OH^-, a water molecule will likely form at the *boundary* of the cavity, which defines the asymmetry. The key is to ask where the excess electron can most easily localize. It makes no sense energetically that the H atom solvation cavity should fully collapse, followed by the creation of a new solvent cavity for the electron. By analogy with the presolvated electron problem, electron localization can most easily occur in a "pre-existing" region of low solvent density: the H-atom cavity. Similar considerations apply to the reverse reaction. Simulations indicate that electrons are solvated on average with one OH bond of each solvating water molecule pointing in toward the negative charge, and the other forming a hydrogen bond to the next solvation shell. In the reaction -14 of an electron with one of these H_2O molecules, an OH bond near the electron charge center can dissociate, leaving a proton to combine with the unpaired electron and to form a hydrogen atom within the pre-existing cavity. This formulation avoids some of the work needed to create a new void in the solution, and requires only rearrangement of the walls of the solvent cage. When these complementary pictures are connected by a common transition state, it becomes clear that in the $(H)_{aq} \rightleftharpoons (e^-)_{aq}$ equilibrium, the unpaired electron does not "move" from the solvent cavity; rather, the transformation is effectively accomplished by *proton transfer* between a water molecule and the nucleophilic electron charge center within the cavity. The energetics and primary isotope effects in the forward and reverse reactions are most easily explained in these terms. A two-dimensional representation of the overall process is shown in Figure 28.

$$H + OH^- \rightleftharpoons (e^-)_{aq} + H_2O$$

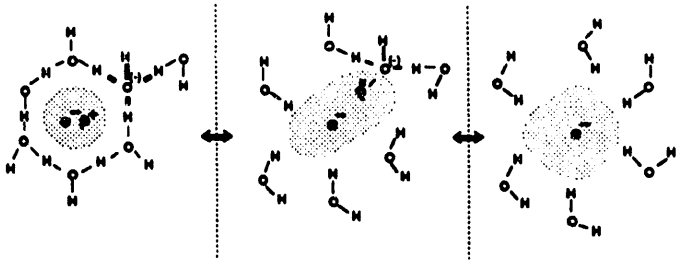

Figure 28. Proton-transfer mechanism envisioned for equilibrium 14.

If proton transfer from water to the solvated electron is possible in the case of reaction -14, there is no reason to think that similar proton-transfer reactions from stronger Bronsted acids should not occur. The most obvious example is the well-known reaction of $(e^-)_{aq}$ with hydronium ion, equation 17.

$$(e^-)_{aq} + (H_3O^+)_{aq} \rightharpoonup (H)_{aq} + H_2O \qquad (17)$$

Reaction 17 is very fast ($k_{17} = 2.3 \times 10^{10}$ M^{-1} sec^{-1}), but five to 10 times less than diffusion limited. The hydronium ion is an exceptionally poor scavenger of presolvated electrons. Thus, like water itself, it has no tendency to act as an excess electron acceptor in an electron-transfer reaction. The properties of reaction 17 can readily be explained in terms of a proton transfer from hydronium to the weak base $(e^-)_{aq}$, but are hard to reconcile with an electron-transfer mechanism.

A number of moderately slow $(e^-)_{aq}$ reactions with Bronsted acids that give H atoms as products can be correlated by a Bronsted plot of reaction rate vs. pK_a. An updated version of this Bronsted plot for hydrated electron reaction with aqueous acids appears in Figure 29. One can probably conclude that all Bronsted acids that are poor electron acceptors will react by proton transfer to $(e^-)_{aq}$ at the minimum rate suggested in this Bronsted correlation.

The possibility of proton transfer to the weak base $(e^-)_{aq}$ may have further interesting implications for the unique bimolecular recombination reaction of two hydrated electrons. Evidence suggests that this reaction occurs by a two-step mechanism, very possibly involving a dielectron, as in equation 18.

$$(e^-)_{aq} + (e^-)_{aq} \rightharpoonup (e^-)^2_{aq} \rightarrow H_2 + 2OH^- \qquad (18)$$

No H atoms are produced in this reaction, which means that spin pairing must occur prior to or in concert with the actual creation of the singlet H_2 molecule. When the spin factor of 1/4 is included in the Debye-Smoluchowski rate expression for diffusion-limited reaction of charged species, one deduces a reaction distance for the hydrated electron pair of approximately 10 Å. This would seem to imply a long-range electron-transfer process, and it is difficult to imagine any "acceptor" site other than the existing hydration cavity of one of the electrons. The isotopic enrichment favoring H over D in the H_2, D_2, and HD product mixture is quite large, suggesting an intermediate that lives long enough (picoseconds?) to thermally equilibrate with protons and deuterons of the solvent. The second-order electron recombination proceeds at a rate that is nearly diffusion limited, below ca. 150 °C. At higher temperatures, the disappearance rate actually decreases, which suggests that the activation energy for the reverse step of the pre-equilibration is much higher than the forward reaction step, and at a sufficiently high temperature the dielectron dissociation competes kinetically with the next step in the reaction. What is the next step? If proton transfer limits the lifetime of the hydrated electron, it may well also limit the (much shorter) lifetime of the hydrated dielectron. Thus, we suggest that a water molecule reacts by proton transfer to the dielectron, forming H^-.

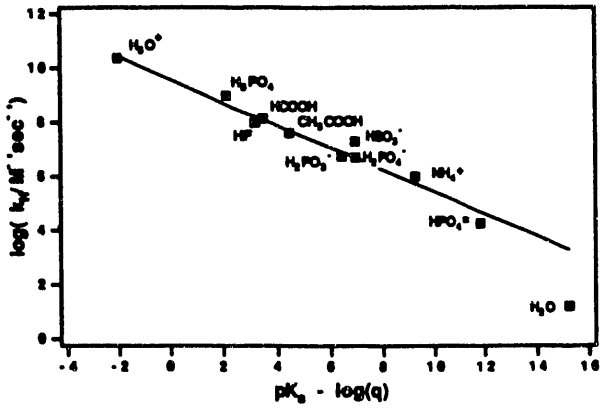

Figure 29. Bronsted correlation of reaction rates and acid/base equilibrium constants for acids that transfer protons to hydrated electrons. The variable q is the number of equivalent proton-accepting sites on the conjugate base. In the case of acetic acid, the rate is corrected to separate the competing electron-attachment and proton-transfer rates.

$$(e^-)^2_{aq} + H_2O \rightarrow H^- + OH^- \quad (19)$$

$$H^- + H_2O \rightarrow H_2 + OH^- \quad (20)$$

The hydride ion then reacts immediately with another water molecule to form H_2, as in the generally accepted "hydride" mechanism for the $H + (e^-)_{aq}$ reaction.

3. Solvent Relaxation Dynamics

Y. Lin, C. D. Jonah

The effects of solvation and solvent dynamics on chemical reactions and, especially, on charge-transfer processes, have long been a subject of great importance in radiation chemistry. In the past, attention was focused primarily on equilibrium solvent effects, such as the effect of solvent polarity on the reaction. Two questions that have only recently come to the forefront in this area of research are, (1) how do solvent molecules react to the sudden creation of a charged species? and (2) how is this response controlled by microscopic factors in the molecular structure of the charged molecule and in the solvent structure. In the past decade, a number of researchers have employed picosecond time-resolved absorption and emission spectroscopy to probe the dynamics of electron solvation or the solvation of a large molecular dipole created in a polar liquid. However, until we began our studies, the solvation dynamics of anions in room-temperature liquids had not been measured. This is a major deficiency because many chemical processes that occur in the condensed phase involve ions or ionic intermediates. The solvation of these charged species can greatly affect chemical events. In fact, prior to our studies, the only information that has been obtained about the anion solvation dynamics has come from trying to understand chemical reactivity in different solvents by using models for the role of solvation on the total reactivity—thus deriving the effect from the consequences. The studies described here focus on the structural and dynamical properties of ion solvation.

a. Ion Solvation and Solvent Structure

Experimental studies of solvation dynamics are usually carried out by instantaneously creating a dipole or charged species in a polar solvent and subsequently monitoring the emission or absorption spectrum of this species. As solvation of this species progresses, the solvent structure rearranges, leading to a change in the energy of the probe molecule or ion that changes the emission or absorption spectrum. We selected the benzophenone anion as the microscopic probe for the following reasons: (1) The anion spectrum is separated from that of the triplet and excited state, and is strongly shifted by a polar solvent. (2) The anion can be produced very quickly by a reaction with the "dry electron", which can conveniently be produced by electron beam radiolysis.

How do the structures of the solvent molecules determine the dynamics and energetics of solvation? We studied the transient absorption spectra of benzophenone anion in linear alcohols, branched alcohols, and acetonitrile. Our results demonstrate that solvent reorganization strongly affects the electronic structure of the solute ions, and changes the absorption spectrum of the ions. Figure 30 shows the benzophenone anion absorption spectrum in n-octanol at 50 ps, 300 ps, and 3 ns after the electron beam pulse. The blue shift of the spectrum is quite obvious. The time-dependent behavior in other alcohols is similar, albeit faster for the smaller alcohols. The absorption maximum of the benzophenone anion spectrum shifts from 675 nm to 635 nm and then to 625 nm for the three different times. The final broad absorption band has been assigned to the relaxed benzophenone anion in alcohol, whereas the spectra at early times are assigned to the anion before solvent rearrangement. As shown in Figure 31, the final absorption peak position and width are practically the same throughout the linear alcohol series. Only the timescale for the blue shift depends on the chain length of the alcohol.

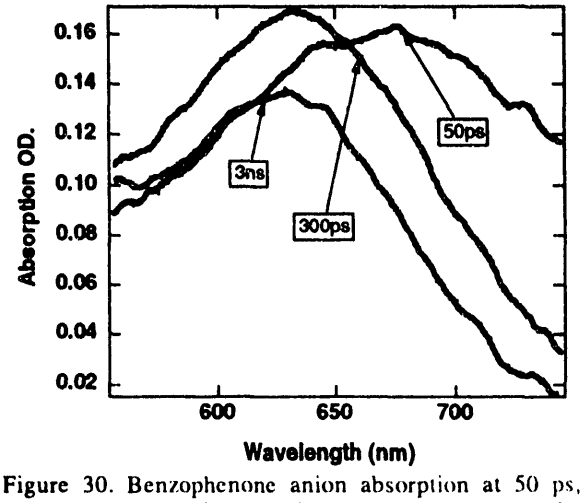

Figure 30. Benzophenone anion absorption at 50 ps, 300 ps, and 3 ns after the electron pulse in n-octanol.

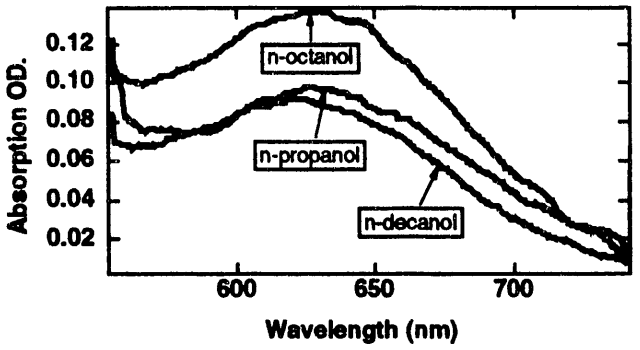

Figure 31. Transient absorption spectra of benzophenone anion in three different linear alcohol solvents (n-propanol, n-octanol, and n-decanol) at 3 ns after the electron pulse.

The situation is very different when the solvent is changed from a linear to a branched alcohol. Figure 32 plots the absorption of the benzophenone anion in n-octanol and 2-octanol. As shown in Figure 32 (top), the absorption spectra are very similar for the primary and secondary alcohols at very early times, times prior to solvation. Both reflect newly created ion species in random (unrelaxed) solvent configurations. The absorption spectra are very different for the fully solvated species in linear and branched alcohols. The shift of the spectrum of the benzophenone anion in 2-octanol is smaller than in n-octanol, and the final spectral position is about 35-nm red-shifted from what is observed in the normal alcohol. Similar solvation behavior was also observed in other branched alcohol systems such as 2-butanol and 2-propanol.

The transient absorption spectra of the benzophenone anion in acetonitrile are shown in Figure 33. The absorption maxima at 50 ps, 300 ps, and 3 ns are the same; unfortunately, the time-dependent solvation process in this system is too fast for us to observe. However, the final position of the anion absorption shows that the equilibrium local solvent structure and energetics in acetonitrile are significantly different from those in linear alcohols. The absorption spectrum at 3 ns is 90-nm red-shifted compared to the linear alcohols and 55-nm red-shifted compared to the branched alcohols. The red shift of the probe absorption spectra in going from linear alcohols to branched alcohols and to acetonitrile was also observed for the solvated electron.

The differences between the primary and secondary alcohols cannot be explained by the concentration of dipoles because the dipole concentrations of n-octanol and 2-octanol are the same. The difference, can,

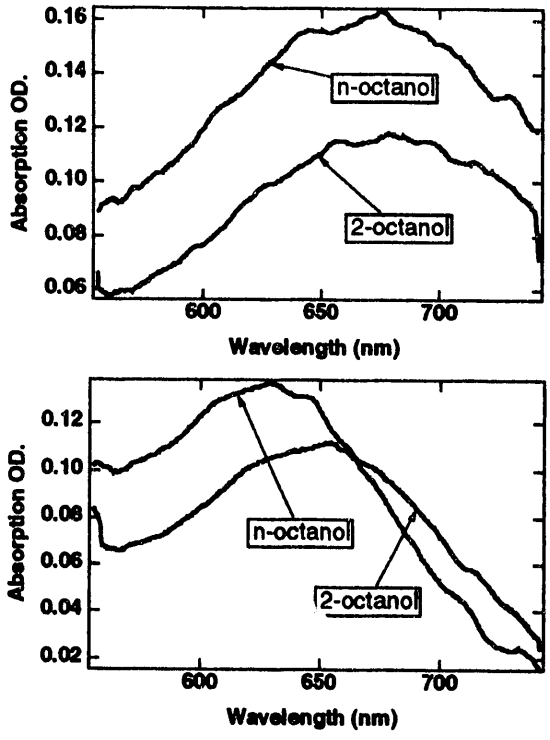

Figure 32. The transient absorption spectra of benzophenone anion in n-octanol and 2-octanol solution at 50 ps (top) and 3 ns (bottom) after the electron pulse.

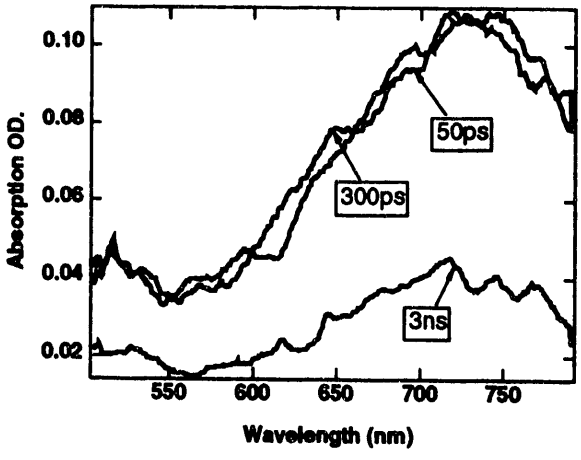

Figure 33. The transient absorption spectra of benzophenone anion in acetonitrile. The center of the absorption peak is at 720 nm.

however, be explained by the steric factors that will prevent a close packing of secondary alcohols around an anion. For a primary alcohol, there is only a single carbon chain attached to the carbon atom bonded to the OH dipole. The OH dipole can point towards the anion and the carbon chain extend in the opposite direction. There will thus be little interference

between alcohol molecules. However, for the secondary alcohol, there are two carbon chains attached to the carbon atom bonded to the OH dipole. The second carbon chain (in the experiments described here, a methyl group) will interfere with a neighboring alcohol molecule, and thus the OH moieties will not be as near to the anion for a secondary alcohol as for a primary alcohol. Modeling studies in support of these ideas are given in the next section.

b. Monte Carlo Simulations of Solvation Energetics

We have used Monte Carlo (MC) simulations to evaluate our hypothesis that the difference between primary and secondary alcohols is due to the differences in the packing of the solvent molecules around an anion. In this simulation, we have used a simplified model that encompasses the linear and branched chain alcohols and acetonitrile within a simple framework and mapped the energetics of the system as a function of the relevant solvent properties.

We have explored the equilibrium properties of the anion solvation process in a model dipolar cluster. The model consists of N solvent molecules around a central charged entity (anion). Studies were done as a function of N ($N \leq 342$), and no significant differences were found. The solvent molecules are assumed to have the shape of three linearly connected hard spheres. Three different dipole distributions of the solvent molecules were used. In the first case, the solvating dipole is at the end of the molecule with its positive charge at the exposed end. This describes the linear alcohols. The second case corresponds to the situation in acetonitrile, where the dipole is at the end of the molecule, and the exposed end is negatively charged. The third case simulates the situation in the branched alcohols, where the dipole is located in the center of the molecule (center ball in our model) and is perpendicular to the axis of the molecule.

The degrees of freedom that are involved in the calculation of the energetics are the position and orientation of the solvent molecules as well as the position and orientation of the solvent dipole moments. All electrostatic interactions among the solvent and solute molecules are considered explicitly. Other molecular interactions are simply replaced by hard-sphere repulsive potentials that keep molecules from overlapping.

The process of "relaxation to equilibrium" was monitored through the calculation of the solvation energy V_S, which is the electrical potential at the solute site. This was done as a function of the number of configurations for several different initial configurations. After the system has reached equilibrium, the values of solvation energy obtained from different initial configurations are within the statistical fluctuation. The influence of the initial configuration disappeared after 30,000 configurations. These calculations have been done for a series of cluster sizes from 26 to 342, and the results were found to be independent of cluster size.

The potential well arising from the arrangement of the solvent molecules around the anion was calculated. The results of these calculations are shown in Figure 34. The differences in the potentials are evident for the three different placements of the dipole group in the model solvent molecule. In these calculations, the central charge is assumed to be the anion. As can be seen in Figure 34, curve 1 (primary alcohols) shows the deepest and narrowest potential well; hence, the absorption of the anion in this kind of solvent would occur at higher energy. This indeed is what we observed experimentally. Curve 2 (acetonitrile) displays a relatively shallow and wide potential well. Curve 3 (branched alcohols) shows a deeper potential than for acetonitrile but the potential is not as narrow nor as deep as curve 1. From Figure 34, red shift is expected to occur on going from linear alcohols to branched alcohols to acetonitrile.

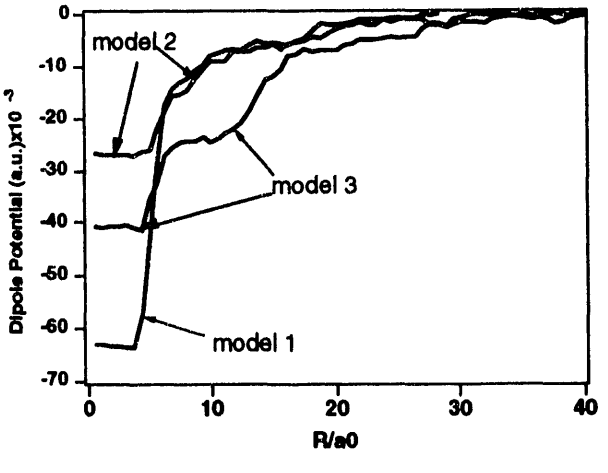

Figure 34. Monte Carlo simulation of the distance dependence of the dipole potential energy for three different model fluids. The parameters used in these calculations are $q_0 = -1$ (a.u.), $p_1 = 1.5$ D, T = 300 K, and N = 124.

Our simulation qualitatively explains the observed spectral shift as a function of solvent, and demonstrates that the charge distribution of the solvent molecules determines the structure and energetics of the solvation process.

c. Solvation Dynamics in Alcohols

To compare the experimental solvation times of the anion and the electron in the same solution, or to relate the solvation times to the solvent dielectric relaxation times, it is necessary to develop an approach to extract solvation parameters from the experimental data. This cannot be done by fitting the decay curve at a given wavelength, because the time dependence of the absorptions are different at different wavelengths. To obtain the desired information, a more complete analytical method for obtaining the solvation time has been developed.

To find the solvation time τ_s, we assume that the anion ground state relaxes exponentially with the characteristic time τ_S. During the solvent reorganization process, the center and width of the anion absorption spectrum can be described by equations 21 and 22,

$$\lambda(t) = \lambda_\infty + (\lambda_0 - \lambda_\infty)e^{-t/\tau_s} \qquad (21)$$

$$\Delta(t) = \Delta_\infty + (\Delta_0 - \Delta_\infty)e^{-t/\tau_s}, \qquad (22)$$

where λ_0 and λ_∞ are the anion absorption maxima for the initial unsolvated species and final solvated species, respectively, and Δ_0 and Δ_∞ are the corresponding absorption band widths. The expressions given in (21) and (22) allow the time- and wavelength-dependent anion absorption to be written as equation 23,

$$I(\lambda,t) = \frac{1}{\sqrt{2\pi}\Delta(t)} e^{-\frac{(\lambda-\lambda(t))^2}{2\Delta^2(t)}} e^{-k_r t} \qquad (23)$$

where k_r is the rate for the subsequent chemical process, such as charge recombination. To accurately obtain the solvation time τ_S, the magnitude of k_r should be small compared to the rate of solvation.

For comparison with the experimental data, equation 23 must be convolved with the instrument response function. The parameters λ_0 and Δ_0 in equation 23 are independently obtained from the absorption of the benzophenone anion in nonpolar solvents (λ_0 = 790 nm, Δ_0 = 105 nm in n-hexane). The value of λ_∞ is obtained from the long time limit of the anion absorption. The parameters left to be determined are Δ_∞, τ_S, and k_r. Because of the early formation of benzophenone triplet and ketyl radical product, Δ_∞ cannot be accurately determined from the final spectrum, so it appears as an adjustable parameter. Figure 35 shows the results of the calculation for the transient absorption data of the benzophenone anion in n-octanol. The parameters, τ_s, Δ_∞, and k_r are listed in Table 5. The Δ_∞ values for three different linear alcohols are very similar. The value of τ_r ($1/k_r$) is ≈3 ns, which is two orders of magnitude longer than the characteristic solvation time (τ_S) in the same solvent. Therefore, the solvation processes we are studying are not influenced by subsequent chemical processes.

It is interesting to compare and contrast the dynamics measured here with those found for electron solvation. The initial solvent arrangement around a benzophenone ion should be favorable for the neutral

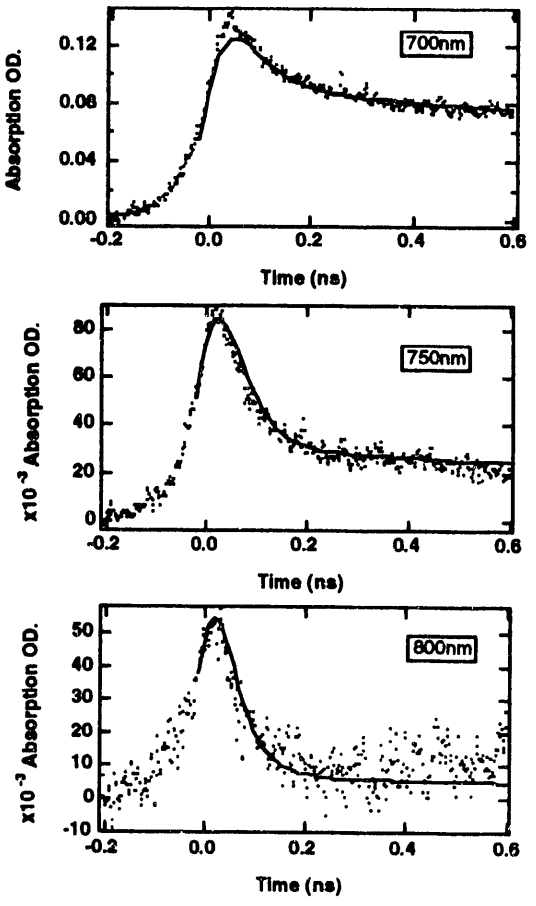

Figure 35. Time-dependent absorption of the benzophenone anion at several different wavelengths in n-octanol. The lines correspond to the calculations from equation 23, and the dots are the experimental data. In these calculations τ_s = 55 ± 5 ps, Δ_∞ = 68 ± 2 nm, and ($1/k_r$) = 2.8 ± 0.3 ns.

Table 5. The characteristic benzophenone anion solvation time τ_s and final spectral bandwidth Δ_∞ in several linear alcohols. The rates for the subsequent chemical reaction are also given for comparison.

Solvents	τ_s(ps)	Δ_∞ (nm)	$\frac{1}{k_r}$ (ns)
n-butanol	35	66	2.0
n-octanol	55	70	2.8
n-decanol	90	70	3.0

benzophenone molecule, whereas the electron solvation begins from a configuration that is particularly favorable for the electron (otherwise the electron would not be trapped in that particular location). To assess these effects and to give an idea of the kind of solvation mechanism that may be operating, we have prepared Table 6 to summarize (1) the benzophenone anion solvation times obtained from this study; (2) the electron solvation times; and (3) solvent dielectric relaxation times. The results indicate that anion solvation is slower than electron solvation. For example, the solvation time for the benzophenone anion in n-decanol is approximately 90 ps, whereas the electron solvation time is 55 ps. These values can be compared to the dielectric relaxation times for n-decanol for τ_1-τ_3 of 2 ns, 48 ps, and 3.3 ps. The three Debye relaxation times τ_1, τ_2, and τ_3 are associated with the time scales of hydrogen-bonding dynamics in molecular aggregates, the molecular rotation, and rotation about the terminal C—OH bond, respectively. For both dipole solvation and electron solvation, the solvation time correlates best with τ_2, the monomer dielectric rotation time of the alcohol.

A more rigorous description can be given by using the longitudinal relaxation time τ_L, which is defined as $(\varepsilon_\infty/\varepsilon_0)\tau_D$, where ε_∞ and ε_0 are the infinite frequency and static dielectric constants, and τ_D is the Debye dielectric relaxation time. Because of the complicated dispersion behavior in alcohols, a single value of τ_L does not exist. The experimentally measured solvation times in alcohol solutions are faster than τ_{L1}, but are slower than τ_{L2}. The observed solvation time is a blend of several solvent motions and a combination of different dielectric relaxation times. Because it takes longer to move an alcohol molecule if a hydrogen bond must be broken, the longer time for the anion solvation suggests that the initial structure around the anion requires a greater rearrangement of the solvent molecules than the structure near an electron, and that part of the reorganization will require the breaking of hydrogen bonds.

d. Dynamics in Salt Solutions

The experiments described above probe the solvation of ions in dipolar, nonconducting solutions. However, in many chemical systems, counterions play an important role in the chemistry. Although ionic effects are well known in chemistry, the quantitative understanding of the role of ions at high concentrations is still fragmentary. This section represents an extension of our studies on solvation dynamics into the realm of ionic solutions. In some ways, ionic solutions might be viewed as simply more polar versions of the pure solvent counterparts. They could, therefore, be expected to influence reactions in a similar manner. Dynamically, however, ionic solutions are very different from pure polar solvents. Whereas dynamics in a pure solvent involves primarily the reorientation of solvent molecules, the time dependence of salt-solute interactions arises from the translational motion of ions.

We have used both picosecond and nanosecond pulse radiolysis techniques to examine the behavior of benzophenone anion in several ionic solutions with Li^+, Na^+, and Ba^{2+} in acetonitrile. Transient absorption spectra of the benzophenone anion in the presence of 0.5 M $NaClO_4$ in acetonitrile are shown in Figure 36. In the absence of salt, the solvation dynamics of the benzophenone anion in acetonitrile are too fast to be observed, and the absorption maximum of the final solvated species is 720 nm. In the

TABLE 6. The benzophenone anion solvation times obtained from this experiment and electron solvation times in several linear alcohol systems. Dielectric data are given for comparison.

solvents	τ_s (ion) (ps)	τ_s (electron) (ps)	dielectric relaxation times (ps) τ_1	τ_2	τ_3	$\tau_{L1} = \tau_1\left(\frac{\varepsilon_{\infty 1}}{\varepsilon_{o1}}\right)$ (ps)	τ_{L2} (ps)
n-butanol	35	30	670	27	2.4	127	21
n-octanol	55	45	1780	39	3.2	406	30
n-decanol	90	51	2020	48	3.3	565	42

presence of 0.5 M $NaClO_4$, the absorption maximum of the radical anion of benzophenone is blue-shifted from 720 nm to 650 nm, and the dynamics are considerably slower. As in the pure solvent, the spectral dynamics cannot be described by a "two-state" kinetic model; instead, the spectral change appears to be continuous as the environment around the benzophenone rapidly alters from the original unstable state to the final state. Figure I-37 shows that solvation is a nanosecond process. The solvation dynamics observed are strongly affected by the identity and the concentration of the cation. The different relaxation times for different cation solutions may indicate strong coupling between the benzophenone anion and a cation, or may indicate the formation of contact ion pairs: benzophenone radical anion-cation.

Two other research groups have recently studied dipole solvation in salt solutions. These experiments show, consistent with our results, that solvation is much slower in ionic solutions and depends on the salts and their concentration in the solution. They have interpreted their results by using two different models, one based on the Debye-Falkenhagen (DF) theory and the second based on specific ionic interactions. Both models appear to be unsatisfactory to explain their observation. The solvent times calculated from DF theory are about an order of magnitude faster than the experimental measurements, whereas the concentration dependence expected from the ionic interactions is not in agreement with the experimental data. We believe that our findings provide a better guide for the interpretation of this family of observations, and we are now studying this important issue.

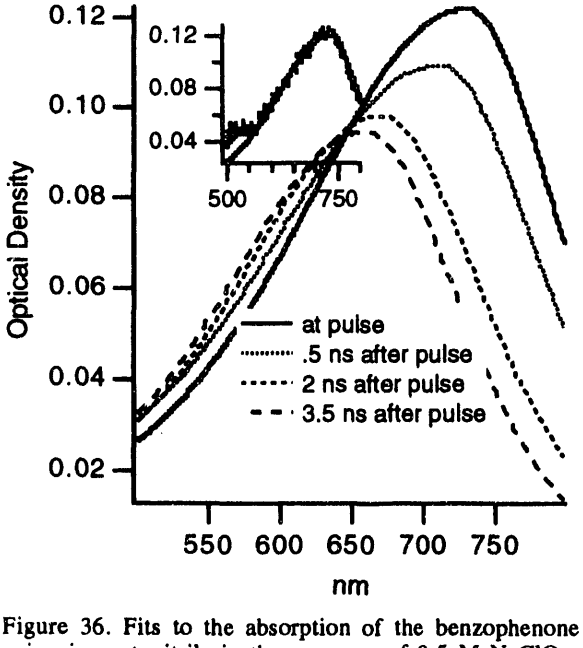

Figure 36. Fits to the absorption of the benzophenone anion in acetonitrile in the presence of 0.5 M $NaClO_4$. The inset shows the experimental data at the pulse end and the fitted absorption. The peak at 550 nm is assigned to the ketyl radical.

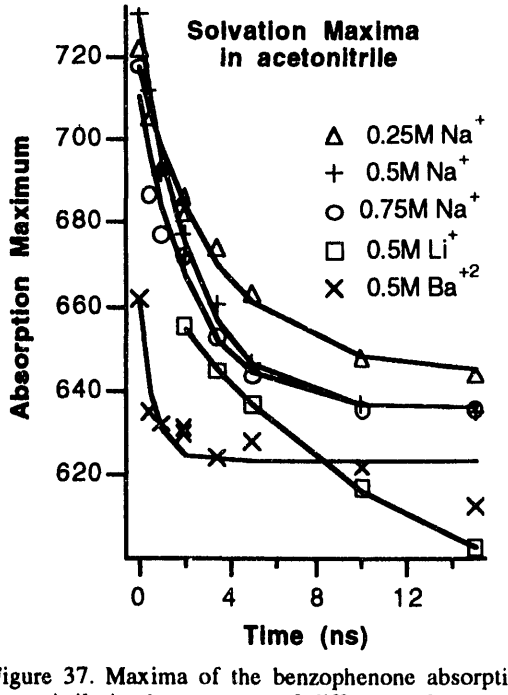

Figure 37. Maxima of the benzophenone absorption in acetonitrile in the presence of different salts at various salt concentrations. Lines are least-squares fits to an exponential decay.

ACCELERATOR ACTIVITIES

C. D. Jonah, B. E. Clifft, G. L. Cox, D. T. Ficht, R. H. Lowers, A. C. Youngs, D. Werst

A. 20-MeV Linac *C. D. Jonah, B. E. Clifft, G. L. Cox, D. T. Ficht*

The safety systems of the linac have been upgraded in both hardware and documentation during the past year. All radiation detectors in user-occupied areas have been replaced with "fail-safe"-type detectors that are suitable for high-peak-pulse machines. In addition, a failure analysis for the interlock systems was done, new operating procedures were written, and new safety systems were installed. The results will appear in the Safety Analysis Report for the linac.

This linac was built in the late 1960s for radiation chemical studies. It is uniquely suited to radiation chemical experiments because both short pulses and high powers are available. The current in the picosecond pulse was increased approximately four-fold in 1978 by modifying the subharmonic bunching to work on the 12th harmonic instead of the sixth harmonic. In the late 1980s, a pulse-compression technique was devised that compressed the electron pulse to 5 ps from 30 ps with the same beam current. Studies are possible ranging over a 5-ps pulse with 6 nC of charge to a 30-ps pulse with 40 nC of charge to a 9-μsec pulse with 10 μC of charge. The energy of the beam, 20-MeV transient mode or 15-MeV steady-state mode, is sufficiently high to easily penetrate a reaction cell or even an oven, but not so high that nuclear activation is a major problem. The machine is currently being used to study the pathways by which kinetic energy is transformed into chemical potential energy, to study electron-transfer reactions, to create and study unusual oxidation states of lanthanides and actinides, and to study unusual short-lived molecules. In addition, scientists from the Advanced Photon Source are using the linac to characterize the impedance of the waveguides and chambers that will make up the light source. These experiments are critical to the design of the APS because the eddy currents induced by the positron beam going through the cavities and chambers of the machine can defocus the positron beam.

B. 3-MeV Van de Graaff Accelerator *R. H. Lowers, A. C. Youngs, D. Werst*

The 3-MeV Van de Graaff accelerator supports the magnetic resonance studies of the Radiation Chemistry and Photochemistry Group. The machine can provide 1-ns to 10-μs pulses of electrons or protons. The low noise of the machine makes it ideal for studying radical processes by using magnetic resonance and optical-magnetic resonance techniques. Such studies are described above.

This year, considerable time has been spent reviewing control and safety systems with the goal of documenting the safety of the system. The activities are very similar to those outlined for the linac. One major study was a maximum credible incident analysis for a gas spill from the Van de Graaff tank.

PUBLICATIONS

ELECTRONIC STATES OF CIS- AND TRANS-DECALIN RADICAL CATIONS IN ZEOLITES
M. V. Barnabas and A. D. Trifunac
Chem. Phys. Lett. 187, 565-570 (1991)

INVESTIGATION OF ELECTRON TRANSFER BETWEEN HEXAARYLBIIMIDAZOLE AND VISIBLE SENSITIZER
Y. Lin, A.-D. Liu, A. D. Trifunac, and V. V. Krongauz
Chem. Phys. Lett. 198, 200 (1991)

H/D ISOTOPE EFFECTS IN WATER RADIOLYSIS. 3. ATOMIC HYDROGEN IN ACIDIC H_2O/D_2O MIXTURES
P. Han and D. M. Bartels
J. Phys. Chem. 95, 9370-9374 (1991)

SOLVENT EFFECTS ON THE PHOTOCHEMISTRY OF A KETOCYANINE DYE AND ITS FUNCTIONAL ANALOGUE, MICHLER'S KETONE
M. V. Barnabas, A. D. Liu, A. D. Trifunac, V. V. Krongauz, and C .T. Chang
J. Phys. Chem. 96, 212-217 (1992)

CONDENSED PHASE STUDIES OF RADICAL IONS IN PHOTOIONIZATION AND RADIOLYSIS
A. D. Trifunac, A.-D. Liu, and D. M. Loffredo
Dynamics and Mechanisms of Photoinduced Transfer and Relate Phenomena, N. Mataga et al., Eds.;
Elsevier Science Publishers, 1992, pp. 259-274

PHOTOIONIZATION OF POLYCYCLIC AROMATIC HYDROCARBONS IN ALKANE SOLUTIONS: "HIGH ENERGY" CHEMICAL PATHWAYS
D. M. Loffredo, A.-D. Liu, and A. D. Trifunac
Rad. Phys. Chem. 40, 255-262 (1992)

PHOTODISSOCIATION OF HEXAARYLBIIMIDAZOLE. II. DIRECT AND SENSITIZED DISSOCIATION
A.-D. Liu, A. D. Trifunac, and V. V. Krongauz
J. Phys. Chem. 96, 207-212 (1992)

ION-MOLECULE REACTIONS OF TETRAMETHYLETHYLENE RADICAL CATIONS IN ZEOLITES
M. V. Barnabas and A. D. Trifunac
Chem. Phys. Lett., 193, 298-304 (1992)

FLUORESCENCE-DETECTED MAGNETIC RESONANCE
D. W. Werst and A. D. Trifunac
Chapter: A Specialist Periodical Report, Electron Spin Resonance, Royal Society of Chemistry,
M. C. S. Symons, Ed., 1992, pp. 161-186

STUDIES OF ION SOLVATION USING PULSE RADIOLYSIS
C. D. Jonah and Y. Lin
Proceedings, 9 ICRR: A Twentieth-Century Perspective, Vol. II, 1992, pp. 63-68

PULSE RADIOLYSIS OF DEXTRAN-WATER SOLUTIONS
M. M. Glezen, A. C. Chernovitz, and C. D. Jonah
J. Phys. Chem. 96, 5180-5183 (1992)

EXPERIMENTAL INVESTIGATION OF THE DYNAMICS OF BENZOPHENONE ANION SOLVATION
C. D. Jonah and Y. Lin
Chem. Phys. Lett. 191, 357-361 (1992)

RADIOLYTIC AND RADIOLYTICALLY INDUCED GENERATION OF GASES IN SIMULATED WASTE SOLUTIONS
D. Meisel, M. C. Sauer, Jr., C. D. Jonah, H. Diamond, M. S. Matheson, F. Barnabas, E. Cerny, and Y. Cheng
Proceedings, Waste Management '92 "Working Towards A Cleaner Environment", March 1-5, 1992, Tucson, AZ, pp. 859-865

H/D ISOTOPE EFFECTS IN WATER RADIOLYSIS IV. THE MECHANISM OF $(H)_{aq} \rightleftharpoons (e^-)_{aq}$ INTERCONVERSION
P. Han and D. Bartels
J. Phys. Chem. 96, 4899-4906 (1992)

TEMPERATURE DEPENDENCE OF SOLVATED ELECTRON DIFFUSION IN H_2O AND D_2O
K. H. Schmidt, P. Han, and D. Bartels
J. Phys. Chem. 96, 198-206 (1992)

RADICAL-CATION COMPLEXES FORMED BY π-LONE PAIR INTERACTIONS
D. W. Werst
J. Phys. Chem. 96, 3640-3646 (1992)

ELECTRON TRANSFER FROM CO_2^- TO PERYLENE IN CYCLOHEXANE
M. C. Sauer, Jr. and C. D. Jonah
J. Phys. Chem. 96, 5872-5875 (1992)

SOLVENT AND ISOTOPE EFFECTS ON ADDITION OF ATOMIC HYDROGEN TO BENZENE IN AQUEOUS SOLUTION
E. Roduner and D. M. Bartels
Ber. Bunsenges. Phys. Chem. 96, 1037 (1992)

DIFFUSION AND CIDEP OF H AND D ATOMS IN SOLID H_2O, D_2O AND ISOTOPIC MIXTURES
D. M. Bartels, P. Han, and P. W. Percival
Chem. Phys. 164, 421 (1992)

TRANSIENT ABSORPTION SPECTRA OF AROMATIC RADICAL CATIONS IN HYDROCARBON SOLUTIONS
A-D. Liu, M. C. Sauer, Jr., D. M. Loffredo, and A. D. Trifunac
J. Photochem. Photobiol. A: Chem. 67, 197 (1992)

OTHER PUBLICATIONS

The following are available from the National Technical Information Service:

RADIATION CHEMISTRY OF SYNTHETIC WASTE
D. Meisel, H. Diamond, E. P. Horwitz, C. D. Jonah, M. S. Matheson, M. C. Sauer, Jr., J. C. Sullivan
ANL-91/40

RADIOLYTIC GENERATION OF GASES FROM SYNTHETIC WASTE ANNUAL REPORT - FY1991
D. Meisel, H. Diamond, E. P. Horwitz, C. D. Jonah, M. S. Matheson, M. C. Sauer, Jr., J. C. Sullivan, F. Barnabas, E. Cerny and Y. D. Cheng
ANL-91/41

GAS GENERATION AND RETENTION IN TANK 101-SY; A SUMMARY OF LABORATORY STUDIES, TANK DATA AND INFORMATION NEEDS
E. C. Ashby, C. D. Jonah, D. Meisel, L. R. Pederson and D. M. Strachan
PNL-8124 AD-940

SUBMISSIONS

EPR MEASUREMENT OF THE REACTION OF ATOMIC HYDROGEN WITH BR^- AND I^- IN AQUEOUS SOLUTION
D. M. Bartels and S. P. Mezyk
J. Phys. Chem. (1992)

QUADRICYCLANE AND NORBORNADIENE RADICAL CATIONS IN SILICALITE: COMPARISON WITH FREON MATRICES
M. V. Barnabas and A. D. Trifunac
J. Am. Chem. Soc. Comm. (1992)

RADICAL CATIONS OF QUADRICYCLANE AND NORBORNADIENE IN POLAR ZSM-5 MATRICES: RADICAL CATION PHOTOCHEMICAL TRANSFORMATIONS WITHOUT PHOTONS
M. V. Barnabas and A. D. Trifunac (1992)
J. Am. Chem. Soc. Comm. (1992)

CHEMICAL CONSEQUENCES OF NON-HOMOGENEOUS ENERGY DEPOSITION BY IONIZING RADIATION
C. D. Jonah
Rad. Protection Dosimetry (1992)

THE DYNAMICS OF ANION SOLVATION IN ALCOHOLS
Y. Lin and C. D. Jonah
Understanding Chemical Reactivity, ed. J. D. Simon, Kluwer Publishers (1992)

EXPERIMENTAL INVESTIGATION OF THE DYNAMICS OF BENZOPHENONE ANION SOLVATION
C. D. Jonah and Y. Lin
Chem. Phys. Lett. (1992)

EARLY EVENTS IN RADIATION CHEMISTRY AND IN PHOTOIONIZATION
A. D. Trifunac, D. M. Loffredo, and A. D. Liu
J. Rad. Phys. Chem. (1992)

OBSERVATION OF AN AROMATIC RADICAL ANION DIMER: $(C_{10}F_8)_2^{\bullet-}$
D. W. Werst
J. Am. Chem. Soc. (1992)

EARLY EVENTS FOLLOWING RADIOLYTIC AND PHOTOGENERATION OF RADICAL CATIONS IN HYDROCARBONS
D. W. Werst and A. D. Trifunac
Radiat. Phys. Chem. (1992)

MECHANISM OF FORMATION OF TRANSIENT AROMATIC RADICAL CATIONS IN ALCOHOLS: LASER FLASH PHOTOLYSIS AND PULSE RADIOLYSIS STUDIES
A.-D. Liu, M. C. Sauer, Jr., C. D. Jonah, and A. D. Trifunac
J. Phys. Chem. (1992)

SUBEXCITATION ELECTRON INTERACTIONS IN RARE GASES: PRODUCTION OF ELECTRONIC EXCITED STATES IN HELIUM OR NEON MIXTURES WITH ARGON, KRYPTON, OR XENON
R. Cooper and M. C. Sauer, Jr.
Phys. Rev. A (1992)

THE DEPENDENCE OF THE BENZOPHENONE-ANION SOLVATION ON SOLVENT STRUCTURE
Y. Lin and C. D. Jonah
J. Phys. Chem. (1992)

PICOSECOND DYNAMICS OF BENZOPHENONE ANION SOLVATION
Y. Lin and C. D. Jonah
J. Phys. Chem. (1992)

SOLVENT EFFECTS IN NONPOLAR SOLVENTS: RADICAL ANION REACTIONS
D. W. Werst
Chem. Phys. Lett. (1992)

ON THE GENERATION OF H_2 FROM FORMALDEHYDE IN BASIC AQUEOUS SOLUTIONS
S. Kapoor, F. Barnabas, C. D. Jonah, M. C. Sauer, Jr. and D. Meisel
J. Am. Chem. Soc. Comm. (1992)

THE DYNAMICS OF ANION SOLVATION IN ALCOHOLS
Y. Lin and C. D. Jonah
"Understanding Chemical Reactivity, John Simon, ed.; Kluwer Pub. (1992)

PRESENTATIONS

DIFFUSION AND SPIN DYNAMICS OF H AND D ATOMS IN ICE
D. M. Bartels
Physics Seminar, Argonne National Laboratory
December 3, 1991

EPR, SPIN DYNAMICS, AND DIFFUSION OF H AND D ATOMS IN WATER AND ICE
D. Bartels
University of Houston, Texas
February 17, 1992

EPR, SPIN DYNAMICS, AND DIFFUSION OF H AND D ATOMS IN WATER AND ICE
D. Bartels
University of Texas at Austin, Texas
February 18, 1992

EPR, SPIN DYNAMICS, AND DIFFUSION OF H AND D ATOMS IN WATER AND ICE
D. Bartels
Texas Technical University, Lubbock, Texas
February 20, 1992

RADIOLYTIC AND RADIOLYTICALLY INDUCED GENERATION OF GAS IN SIMULATED MIXED WASTE SOLUTIONS
D. Meisel, H. Diamond, C. D. Jonah, M. C. Sauer, Jr., J. C. Sullivan, F. Barnabas, E. Cerny, Y.-D. Cheng
Waste Management '92 Conference, Tucson, AZ
March 1-5, 1992

TRACK STRUCTURE FROM LOW LET RADIATION
C. D. Jonah
Radiation Research Society - 40th Annual Meeting, Salt Lake City, Utah
March 14-18, 1992

HIGH ENERGY CHEMISTRY: RADICAL CATIONS IN RADIOLYSIS AND IN PHOTOIONIZATION
A. D. Trifunac
Invited Speaker, University of Saskatchewan, Saskatoon, CANADA
March 14-20, 1992

INTRODUCTION TO RADIATION CHEMISTRY: CHEMICAL PERSPECTIVE
A. D. Trifunac
Invited Speaker, University of Saskatchewan, Saskatoon, CANADA
March 14-20, 1992

EARLY EVENTS FOLLOWING RADIOLYTIC AND PHOTOGENERATION OF RADICAL CATIONS IN HYDROCARBONS
D. W. Werst and A. D. Trifunac, invited talk
International Conference on Radiation-Tolerant Scintillators and Detectors, Tallahassee, FL
April 28 - May 2, 1992

RADICAL IONS IN RADIATION CHEMISTRY AND IN PHOTOIONIZATION: HIGH-ENERGY CHEMISTRY
A. D. Trifunac, invited speaker
75th Canadian Chemical Conference and Exhibition, Edmonton, Alberta, Canada
May 31-June 4, 1992

ION-MOLECULE REACTIONS INITIATED BY LASER PHOTOIONIZATION OF POLYCYCLIC AROMATIC HYDROCARBONS IN ALKANE SOLUTION
D. M. Loffredo, A.-D. Liu, A. D. Trifunac
25th Great Lakes Regional Meeting, Milwaukee, Wisconsin
June 1-3, 1992

EPR STUDY OF RADICAL CATION REACTIONS IN ZEOLITES
M. V. Barnabas and A. D. Trifunac
25th Great Lakes Regional Meeting, Milwaukee, Wisconsin
June 1-3, 1992

HYDROCARBON RADICAL CATIONS IN ZEOLITES
M. V. Barnabas and A. D. Trifunac
Gordon Conference on Radical Ions, Wolfeboro, NH
June 22-26, 1992

INTERACTIONS OF HYDROCARBON RADICAL CATIONS IN ZEOLITES
M. V. Barnabas and A. D. Trifunac
Gordon Conference on Radiation Chemistry, Newport, RI
July 5-10, 1992

HIGH ENERGY CHEMISTRY
A. D. Trifunac, invited talk
Gordon Conference on Radiation Chemistry, Newport, RI
July 5-10, 1992

EPR OBSERVATIONS OF TRAPPED HOLES ON TiO_2 COLLOIDS
K. R. Cromack, O. I. Micic, Y. N. Zhang, A. D. Trifunac and M. C. Thurnauer
Gordon Conference on Radiation Chemistry, Newport, RI
July 5-10, 1992

HYDROGEN GENERATION FROM THERMAL REACTIONS OF RADIOLYTIC DEGRADATION PRODUCTS OF CHELATORS
S. Kapoor, F. Barnabas, Y. Vojta, C. Jonah, M. Sauer, Jr. and D. Meisel
Gordon Conference on Radiation Chemistry, Newport, RI
July 5-10, 1992

THERMODYNAMIC AND TRANSPORT PROPERTIES OF THE HYDRATED ELECTRON
D. B. Bartels, invited talk
Gordon Conference on Radiation Chemistry, Newport, RI
July 5-10, 1992

THE DYNAMICS OF ANION SOLVATION IN ALCOHOLS - A PULSE RADIOLYSIS STUDY
Yi Lin and C. D. Jonah
Gordon Conference on Radiation Chemistry, Newport, RI
July 5-10, 1992

QUANTUM YIELDS OF AROMATIC RADICAL CATIONS IN ALCOHOLS - LASER FLASH PHOTOLYSIS STUDY
A-D. Liu, D. Loffrado and A. D. Trifunac
Gordon Conference on Radiation Chemistry, Newport, RI
July 5-10, 1992

TIME DEPENDENCES OF G-VALUES OF ANIONS, EXCITED SINGLETS, AND TRIPLETS OF AROMATIC SOLUTES IN ALKANE LIQUIDS
M. C. Sauer, Jr. and C. D. Jonah
Gordon Conference on Radiation Chemistry, Newport, RI
July 5-10, 1992

SOLVENT EFFECTS ON RADICAL ION REACTIONS
D. Werst
Gordon Conference on Radiation Chemistry, Newport, RI
July 5-10, 1992

THE DYNAMICS OF ANION SOLVATION IN ALCOHOLS - A PULSE RADIOLYSIS STUDY
Yi Lin and C. D. Jonah
Gordon Conference on Water and Aqueous Solutions, Plymouth, NH
August 2-7, 1992

EPR, SPIN DYNAMICS AND DIFFUSION OF H AND D ATOMS IN WATER AND ICE
D. M. Bartels, P. Han, P. Percival, E. Roduner
Gordon Conference on Water and Aqueous Solutions, Plymouth, NH
August 2-7, 1992

HIGH-ENERGY CHEMISTRY
A. D. Trifunac
Invited Speaker, Institute of Nuclear Research, Shanghai, China
September 7, 1992

RADICAL CATIONS IN ZEOLITES
A. D. Trifunac
Invited Speaker, Institute of Nuclear Research, Shanghai, China
September 7, 1992

EARLY EVENTS IN RADIATION CHEMSITRY AND IN PHOTOIONIZATION
A. D. Trifunac
Invited Speaker, 8th International Meeting on Radiation Processing; Beijing, China
September 13-18, 1992

CHEMICAL CONSEQUENCES OF NON-HOMOGENEOUS ENERGY DEPOSITION BY IONIZING RADIATION
C. D. Jonah
Invited Speaker, 11th Symposium on Microdosimetry; Gatlinburg, TN
September 13-18, 1992

RADICAL ION PROBES OF SOLVENT EFFECTS IN NONPOLAR LIQUIDS
D. W. Werst
Invited Speaker, University of Alabama, Tuscaloosa
September 24, 1992

COLLABORATIONS

R. Cooper, University of Melbourne, Australia
Studies of transient species created in gases, liquids, and solids are being carried out. Recent efforts have concentrated on the spectra and dynamics of excited species created in solids, such as sapphire, which are investigated via time-resolved measurements of emitted light using the techniques of pulse radiolysis and laser flash photolysis. Sapphire is a prime contender for a lining material of the containment vessel in fusion reactors, and these studies are useful in understanding radiation effects.

V. V. Krongauz, DuPont de Nemours Company, Inc., Wilmington, DE
Several related efforts using laser flash photolysis, EPR, and picosecond laser techniques are being carried out to study the photochemistry of photopolymer initiation. Emphasis has been on the dissociation mechanism of the free-radical initiator HABI (hexaarylbiimidizole) and the role of dye sensitizers.

S. Mezyk, Atomic Energy of Canada, Ltd., Pinawa
Reaction rates of H atoms with and other iodine-containing solutes are being measured for the purpose of predicting the spread of radioactive iodine in potential nuclear accidents.

P. W. Percival, Simon Fraser University and TRIUMF, Burnaby, British Columbia, Canada
Investigation of H and D atoms in ice by time-resolved EPR has allowed determination of diffusion rates, and the development of a model H atom-H_2O interaction potential. The aim of the collaboration is improved understanding of H-atom transport and reactivity in solid lattices.

E. Roduner, Physical Chemistry Institute, Zurich University, Switzerland
Reaction of H atoms with benzene in water has been investigated in a test of the validity of transition state theory for reactions in aqueous solution. Precision measurements of the hyperfine coupling of H and D atoms in water have been made to elucidate the nature of hydrophobic hydration, and effects of water "structure" on reaction rates.

C. Romero, University of Santiago, Chile
The properties of the hydrated electron are being studied via molecular dynamics simulations. A computational program has been developed to simulate aqueous LiCl solutions, and the results are compared to the experimental optical absorption spectrum. Water molecules are treated classically, and the electron is given a full quantum treatment. This is an important step towards simulating chemical reactions in ionic solutions.

END

DATE FILMED

2/10/93